Journal of Computational Physics 228 (2009) 7742–7770

Contents lists available at ScienceDirect

Journal of Computational Physics

journal homepage: www.elsevier.com/locate/jcp

# Calculations of two-fluid magnetohydrodynamic axisymmetric steady-states

N.M. Ferraro *, S.C. Jardin

*Princeton Plasma Physics Laboratory, Princeton, NJ 08543-0451, United States*

ARTICLE INFO

*Article history:*
Received 7 January 2009
Received in revised form 2 June 2009
Accepted 19 July 2009
Available online 26 July 2009

*PACS:*
52.30.Ex
52.55.Fa
52.65.Kj

*Keywords:*
Magnetohydrodynamics
Equilibria
Simulation

ABSTRACT

M3D-C[1] is an implicit, high-order finite element code for the solution of the time-dependent nonlinear two-fluid magnetohydrodynamic equations [S.C. Jardin, J. Breslau, N. Ferraro, A high-order implicit finite element method for integrating the two-fluid magnetohydrodynamic equations in two dimensions, J. Comp. Phys. 226 (2) (2007) 2146–2174]. This code has now been extended to allow computations in toroidal geometry. Improvements to the spatial integration and time-stepping algorithms are discussed. Steady-states of a resistive two-fluid model, self-consistently including flows, anisotropic viscosity (including gyroviscosity) and heat flux, are calculated for diverted plasmas in geometries typical of the National Spherical Torus Experiment (NSTX) [M. Ono et al., Exploration of spherical torus physics in the NSTX device, Nucl. Fusion 40 (3Y) (2000) 557–561]. These states are found by time-integrating the dynamical equations until the steady-state is reached, and are therefore stationary or statistically steady on both magnetohydrodynamic and transport time-scales. Resistively driven cross-surface flows are found to be in close agreement with Pfirsch-Schlüter theory. Poloidally varying toroidal flows are in agreement with comparable calculations [A.Y. Aydemir, Shear flows at the tokamak edge and their interaction with edge-localized modes, Phys. Plasmas 14]. New effects on core toroidal rotation due to gyroviscosity and a local particle source are observed.



## 1. Introduction

It is known that static toroidal equilibria are unstable to rotation [4], and therefore flows will be present in the steady-state. While the magnetostatic equilibrium of magnetically confined fusion plasmas are relatively insensitive to the flows, the stability and transport properties of the plasma may be strongly affected by them [5–7]. Recently, it has been found that strong flows at the plasma edge are stabilizing to resistive wall modes [8,9] and are correlated with the important L–H transition in tokamaks [10]. Also, it is thought that flow shear may significantly reduce transport due to turbulence by suppressing eddy formation [11,12]. Therefore it is desirable to develop a method for obtaining steady-states with flow self-consistently included. Here we focus on obtaining axisymmetric steady-states of a two-fluid plasma model with flow, which may then be used as the basis for three-dimensional stability calculations.

One approach to the numerical calculation of self-consistent steady-states is to cast the stationary ideal magnetohydrodynamic (MHD) equations in terms of free functions of the poloidal flux. In the absence of flows this approach yields the Grad–Shafranov (GS) equation, where the free functions are the pressure and $I = RB_\varphi$, the major radius times the toroidal component of the magnetic field. In the presence of flows, the Grad–Shafranov–Bernoulli equations are obtained, in which case the free functions are more complicated combinations of physical variables, and are not necessarily continuous. Because

* Corresponding author. Present address: General Atomics, La Jolla, CA 92186, United States. Tel.: +1 858 455 2847.
*E-mail address:* ferraro@fusion.gat.com (N.M. Ferraro).

0021-9991/$ - see front matter © 2009 Elsevier Inc. All rights reserved.
doi:10.1016/j.jcp.2009.07.015

the equilibrium solutions to ideal MHD (with or without flow) are not uniquely determined by boundary conditions [13], the solutions obtained by these methods requires specification of various free functions *a priori* (by using empirical profiles, for example). Therefore it is more accurate to say that this method "reconstructs" rather than "predicts" the stationary states. This approach has not been extended to include resistive or viscous effects, or sources, though efforts have been made to include two-fluid effects [14,15]. The numerical codes CLIO [16], FINESSE [17], and FLOW [18] have been developed using such a method to obtain the stationary equilibria of ideal MHD with flow. CLIO and FLOW have been used to reconstruct such stationary states for JET and NSTX-geometry plasmas, respectively [16,19].

A more physically motivated method is to evolve numerically the dynamical equations from some initial condition until a steady-state is reached. This method has several advantages over solving the time-independent equations directly for the equilibrium. First, this method readily admits the inclusion of dissipative and other more complicated terms relatively easily and generally without any algorithmic changes. Second, the same method may be used to observe and investigate the dynamics of the plasma evolution and oscillations in the steady-state which, by definition, are precluded by the GS approach. The main disadvantage of this method is the relatively large amount of processing time that must be spent to arrive at a steady-state when multiple time-scales are present. With this method, the possibility also exists that no stationary steady-states are accessible from a given set of initial conditions; instead, the steady-state could resemble a limit cycle (as has been found to be the case in three-dimensional nonlinear resistive MHD simulations [20]). This approach was taken by Aydemir, who has recently obtained quasi-steady-states of a visco-resistive single-fluid model in low-$\beta$ plasmas (where $\beta$ is the ratio of thermal pressure to magnetic pressure) using the numerical code CTD [21,3].

We employ this initial-value approach to obtain true steady-states of the two-fluid magnetohydrodynamic (MHD) equations, including resistivity, viscosity, gyroviscosity, and particle sources, at realistic values of $\beta$. The numerical code we describe here, M3D-$C^1$, has been significantly extended from what has been described in previous publications [1,22], and is now able to perform calculations in axisymmetric toroidal geometry. In order to obtain the steady-state efficiently, M3D-$C^1$ makes use of a semi-implicit split time step algorithm which is similar to that used in the nonlinear MHD code NIMROD [23] and is numerically stable for values of the time step far in excess of the Courant condition. Spatial discretization is accomplished by the use of triangular $C^1$ finite elements [24] on a fully unstructured mesh. The use of $C^1$ elements allows the efficient implementation of a flux/potential scalar representation of the velocity and magnetic fields. This representation has a number of advantages over coordinate component representation, including the automatic enforcement of $\nabla \cdot \mathbf{B} = 0$ and the ability to calculate incompressible modes accurately. Furthermore, physically meaningful, energy conserving subsets of the fluid equations (such as reduced MHD) may be obtained simply from the full set of equations when written in the flux/potential representation.

The two-fluid model currently implemented in M3D-$C^1$ is described in Section 2. The time-stepping algorithm and spatial discretization scheme are described in detail in Section 3.1, along with some comparisons with other similar methods. In Section 4, calculated steady-states of the two-fluid model with magnetic geometry and $\beta$ typical of an NSTX [2] discharge are presented.

## 2. Model

The following dissipative two-fluid model is implemented in M3D-$C^1$. Unless otherwise noted, all quantities hereafter are normalized using the system of natural Alfvénic units described in Appendix A.

$$\frac{\partial n}{\partial t} + \nabla \cdot (n\mathbf{u}) = \Sigma \tag{1}$$

$$n\left(\frac{\partial \mathbf{u}}{\partial t} + \mathbf{u} \cdot \nabla \mathbf{u}\right) = \mathbf{J} \times \mathbf{B} - \nabla p - \nabla \cdot \Pi + n\mathbf{g} - \Sigma \mathbf{u} \tag{2}$$

$$\frac{1}{\Gamma - 1}\left[\frac{\partial p_e}{\partial t} + \nabla \cdot (p_e \mathbf{u})\right] = -p_e \nabla \cdot \mathbf{u} + \frac{d_i}{n}\left(\frac{n\nabla T_e}{\Gamma - 1} - T_e \nabla n + \mathbf{R}\right) \cdot \mathbf{J} + d_i \Pi_e : \nabla \frac{\mathbf{J}}{n} + Q_\Delta - \nabla \cdot \mathbf{q}_e \tag{3}$$

$$\frac{1}{\Gamma - 1}\left[\frac{\partial p}{\partial t} + \nabla \cdot (p\mathbf{u})\right] = -p\nabla \cdot \mathbf{u} + \frac{d_i}{n}\left(\frac{n\nabla T_e}{\Gamma - 1} - T_e \nabla n + \mathbf{R}\right) \cdot \mathbf{J} + d_i \Pi_e : \nabla \frac{\mathbf{J}}{n} - \Pi : \nabla \mathbf{u} + \frac{1}{2}\Sigma u^2 - \nabla \cdot \mathbf{q} \tag{4}$$

$$\frac{\partial \mathbf{B}}{\partial t} = -\nabla \times \mathbf{E}. \tag{5}$$

The fields being advanced are the density $n$ (quasineutrality is assumed, so $n = n_e = n_i$), fluid velocity $\mathbf{u}$, pressure $p$, electron pressure $p_e$, and the magnetic field $\mathbf{B}$. Temperatures are defined by $T_e = p_e/n$ and $T_i = p_i/n$. The current density $\mathbf{J}$ and electric field $\mathbf{E}$ are defined by

$$\mathbf{J} = \nabla \times \mathbf{B} \tag{6}$$

$$\mathbf{E} + \mathbf{u} \times \mathbf{B} = \eta \mathbf{J} + \frac{d_i}{n}(\mathbf{J} \times \mathbf{B} - \nabla p_e - \nabla \cdot \Pi_e). \tag{7}$$

Here $d_i = c/L_0\omega_{pi}$ (in cgs units) is the normalized collisionless ion skin depth, with the characteristic ion plasma frequency $\omega_{pi} = \sqrt{4\pi n_0 e^2/m_i}$ (also in cgs units). The adiabatic index is $\Gamma$, which is typically 5/3, but which may be used to enforce an isothermal equation of state by letting $\Gamma = 1$. The right side of the particle conservation equation takes the form $\Sigma = \sigma + \nabla\cdot(D_n\nabla n)$, where the particle source $\sigma$ is an arbitrary scalar field. The scalar $D_n$ is an "anomalous" diffusion coefficient, which both improves numerical stability and allows for the modeling of enhanced rates of particle transport due to micro-turbulent effects not otherwise present in our model or resolved in our simulations. The collisional force considered here is the frictional force,

$$\mathbf{R} = \frac{n}{d_i}\eta\mathbf{J}, \tag{8}$$

where the resistivity $\eta$ is implemented as an arbitrary scalar field. In the applications presented here, the resistivity is always taken to have the Spitzer form

$$\eta = \eta_0/T_e^{3/2}, \tag{9}$$

with $\eta_0$ left as an arbitrary constant.

The pressure tensor is taken to have the form $\Pi = \Pi_\circ + \Pi_\wedge + \Pi_\parallel$, where the components $\Pi_\parallel$ and $\Pi_\wedge$ of the pressure tensor $\Pi$ are respectively Braginskii's form of the parallel ion viscosity and ion gyroviscosity [25]. $\Pi_\circ$ is a generic isotropic viscosity.

$$\Pi_\parallel = \frac{\mu_\parallel}{2}(\mathbf{b}\cdot\mathsf{W}\cdot\mathbf{b})(\mathsf{I} - 3\mathbf{bb}) \tag{10}$$

$$\Pi_\wedge = \frac{d_i p_i}{4B}\{\mathbf{b}\times\mathsf{W}\cdot(\mathsf{I} + 3\mathbf{bb}) + [\mathbf{b}\times\mathsf{W}\cdot(\mathsf{I} + 3\mathbf{bb})]^\top\} \tag{11}$$

$$\Pi_\circ = -\mu(\nabla\mathbf{u} + \nabla\mathbf{u}^\top) - 2(\mu_c - \mu)\,\mathsf{I}\,\nabla\cdot\mathbf{u}. \tag{12}$$

Here $\mathbf{b} = \mathbf{B}/B, B = |\mathbf{B}|$, and $\nabla\mathbf{u}^\top$ is the transpose of $\nabla\mathbf{u}$. The rate-of-strain tensor is

$$\mathsf{W} = \nabla\mathbf{u} + \nabla\mathbf{u}^\top - \frac{2}{3}\,\mathsf{I}\,\nabla\cdot\mathbf{u}. \tag{13}$$

The coefficients $\mu_\parallel, \mu$, and $\mu_c$ are implemented as arbitrary scalar fields. The choice of values for the general dissipative viscosity coefficients $\mu$ and $\mu_c$ is constrained by the positivity conditions $\mu > 0$ and $\mu_c > (2/3)\mu$. The heat flux densities take the form

$$\mathbf{q}_e = -\kappa_\circ\nabla T_e - \kappa_\wedge\mathbf{b}\times\nabla T_e - \kappa_\parallel\mathbf{bb}\cdot\nabla T_e \tag{14}$$

$$\mathbf{q} = -\kappa_\circ\nabla T - \kappa_\wedge\mathbf{b}\times\nabla T - \kappa_\parallel\mathbf{bb}\cdot\nabla T, \tag{15}$$

where $\kappa_\circ, \kappa_\wedge$, and $\kappa_\parallel$ are implemented as arbitrary scalar fields.

The electron pressure tensor is taken to have essentially the form of electron viscosity, $\Pi_e = \lambda n\nabla\mathbf{J}$, with $\lambda$ an arbitrary scalar constant. This term improves numerical stability because its inclusion in Eq. (7) leads to a biharmonic operator on the magnetic field in Eq. (5), and thus $\lambda$ may be called a "hyper-resistivity." The physical effect of electron viscosity is very small in the applications of interest here, and scale-lengths associated with this effect are generally below what is resolvable by our spatial discretization. Therefore we use $\lambda$ only to force $\mathbf{J}$ to remain smooth on the spatial discretization scale $\delta x$, and assume that the physically "correct" solution is obtained in the limit $\lambda \to 0$ and $\delta x \to 0$.

The gravitational force takes the form

$$\mathbf{g} = -\frac{g_R}{R^2}\nabla R - g_Z\nabla Z. \tag{16}$$

This term is explicitly given this form rather than left general in order to improve the accuracy and stability of the semi-implicit time step algorithm in cases in which gravitationally driven instabilities are present.

## 3. Numerical methods

### 3.1. Finite elements

Reduced quintic finite elements are used in M3D-$C^1$. These elements are triangular, fifth-order bivariate polynomial elements, constrained to enforce continuity of values and first-derivatives across element boundaries (this is the $C^1$ property).

These finite elements have the advantage of having only three degrees of freedom per node per field asymptotically [24], which leads to a highly compact matrix representation of the discretized equations.

The discretized equations are obtained by application of the Galerkin method. For example, the continuous equation

$$\frac{\partial \nabla^2 U}{\partial t} = \nabla^2(\mu \nabla^2 U) \tag{17}$$

is discretized into the system of equations obtained by representing $U$ as a linear combination of the basis functions $\{v\}$,

$$U(\mathbf{x}, t) = \sum_j U_j(t) v_j(\mathbf{x}), \tag{18}$$

and integrating over the computational domain to obtain

$$-\sum_j \frac{\partial U_j}{\partial t} \int dA\ \nabla v_i \cdot \nabla v_j = \sum_j U_j \int dA\ \mu \nabla^2 v_i \nabla^2 v_j, \tag{19}$$

after integrating by parts. Due to the $C^1$ property of the reduced quintic elements, the second derivative of the finite element representation of any field remains well-defined even at element boundaries, and so Eq. (19) may be computed directly. Therefore, physical equations containing up to fourth derivatives may be computed directly using $C^1$ elements. In contrast, in the case of $C^0$ elements, for which only the first derivative is well-defined at element boundaries, the calculation of this equation would require the introduction of a new equation to define an auxiliary variable $\varpi = \nabla^2 U$, e.g.,

$$\sum_j \varpi_j \int dA\ v_i v_j = -\sum_j U_j \int dA\ \nabla v_i \cdot \nabla v_j.$$

$$\sum_j \frac{\partial U_j}{\partial t} \int dA\ \nabla v_i \cdot \nabla v_j = \sum_j \varpi_j \int dA\ \nabla v_i \cdot \nabla(\mu v_j)$$

For an implicit time step, these two equations would have to be solved simultaneously in a single matrix equation, thereby doubling the rank of the matrix.

One possible disadvantage of $C^1$ elements is that it is likely more difficult to obtain accurate solutions which contain shocks or other discontinuities with these elements. This is because $C^1$ elements are more prone to overshoot and to problems associated therewith (e.g. preserving the positivity of particle density or temperature). In principle, these problems may be mitigated or overcome with aggressive mesh packing in the region of a discontinuity, at some added computational expense. It has been shown that the stationary flows in tokamak geometry may be discontinuous in cases with strongly driven flows (by neutral beams, for example) or very low edge temperatures (and hence low sound speeds) [26,18]. However, these possible issues with $C^1$ elements do not result in any difficulties for the cases considered below, in which flows are everywhere both subsonic and sub-Alfvénic, and shocks are neither expected nor observed to form.

#### 3.1.1. Surface terms

In the preceding example, the surface terms arising from the integrations by parts have been dropped. In the simulations presented here, which have rectangular boundaries aligned with the physical coordinates $R$ and $Z$, these surface terms will vanish identically when Dirichlet boundary conditions are applied. The reason for this is as follows. Consider the term

$$\int dA\ \nabla \cdot (v_i \nabla U) = \sum_j U_j \oint d\ell\, v_i\, \hat{\mathbf{n}} \cdot \nabla v_j \tag{20}$$

where we have used Eq. (18) and Stokes' theorem. Here $\hat{\mathbf{n}}$ is the outward normal vector to the domain boundary. This surface integral can be decomposed into a sum of integrals over each element edge lying on the domain boundary. For any such edge, where it is also true that the edge lies on a line of constant $R$ or $Z$, only six of the basis functions $v_i$ are nonzero anywhere on the edge. These nonzero basis functions are the only ones for which $U$, $\partial_t U$, and $\partial_t^2 U$ are nonzero on the vertices at the endpoints of the edge [24]. (Here $t$ represents the direction tangent to the edge.) Thus, the surface terms are only nonzero in the equations which determine $U$, $\partial_t U$, or $\partial_t^2 U$ on the boundary. It is precisely these equations which are overwritten when Dirichlet boundary conditions are imposed. Therefore, when the boundaries are aligned with the global coordinates $(R, Z)$, and Dirichlet boundary conditions are imposed, the surface terms make no contribution. These conditions are satisfied in all of the simulations considered below. We have verified that simulations with and without some of the surface terms included yield identical results.

This justification for dropping surface terms only holds in the case where the simulation domain boundaries are rectangular and are exactly aligned with the $(R, Z)$ coordinates. When this is not the case, basis functions other than the ones mentioned above may be nonzero on the boundary, and therefore equations which are not overwritten by boundary conditions may also receive contributions from surface terms. Future versions of M3D-$C^1$ will have all surface terms included so that non-aligned and non-rectangular boundaries are treated correctly.

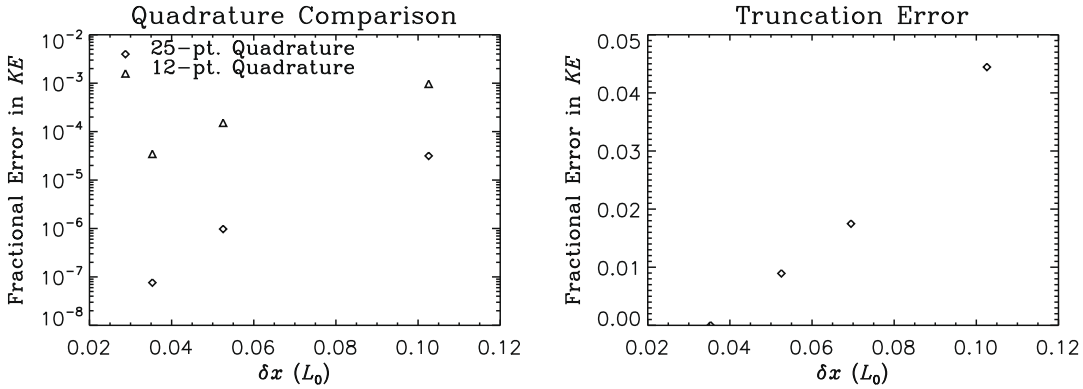


**Fig. 1.** The fractional error in the kinetic energy, as calculated by $\langle |E - E_0| \rangle_t / \langle E_0 \rangle_t$, due to quadrature error (left) and spatial discretization truncation (right). In the quadrature comparison, $E_0$ is the kinetic energy time series calculated using the 79-point quadrature at various mesh resolutions ($\delta x$), and $E$ is the time series at the same resolutions using lower-order quadratures. In the truncation error plot, all results are calculated using the 79-point quadrature, with $E_0$ calculated at $\delta x \approx 0.03 L_0$, and $E$ calculated at various coarser resolutions. The simulations were run for 500 Alfvén periods.

### 3.1.2. Numerical integration

In M3D-C$^1$, spatial integration is now carried out numerically, not analytically as in previous work [1,22]. Analytic integration, while computationally competitive when using a structured mesh in Cartesian geometry, is not feasible on an unstructured mesh in toroidal geometry where the Jacobian of the transformation from each element's local coordinates to the global coordinate system is generally different for each element. The numerical integration is done using Gaussian quadrature with weights and sampling points given by Dunavant [27]. Simulation results presented here have been obtained using a 79-point quadrature. This quadrature is exact for polynomials of up to degree 25, and is therefore exact for discretized nonlinear products of up to four fields when represented using the reduced quintic elements (the integrand being the product of four fields and one basis function, each represented by a degree-five polynomial). The 25-point quadrature, though not exact for highly nonlinear terms, is found to be highly accurate even for relatively coarse meshes. The fractional mean differences between the kinetic energy time series obtained with the 79-point quadrature and those obtained with the 25-point and 12-point quadratures are shown in Fig. 1, for a typical NSTX simulation case. The numerical error introduced by using lower-order quadratures as low as 12-points in this case is found to be smaller than that introduced by the finite element discretization.

## 3.2. Linear semi-implicit time step

The velocity advance is obtained by taking the $\theta$-advanced time discretization of Eq. (2), dropping terms of order $\delta t^2$, and then using Eqs. (5) and (4) evaluated with the $\theta$-advanced $\mathbf{u}$ to eliminate the advanced-time instances of $\mathbf{B}$ and $p$ [28,29]. (By $\theta$-advanced is meant $\mathbf{u} \to \mathbf{u}^n + \theta\,\delta t\,\dot{\mathbf{u}}^n$, for example, where superscripts index the discretized time coordinate.) This procedure results in the following discretization:

$$\begin{aligned} &V_{\mathbf{u}n}(\mathbf{u}^{n+1}, n^m) - \theta\,\delta t[V_{\mathbf{uu}n}(\mathbf{u}^{n+1}, \mathbf{u}^n, n^m) + V_{\mathbf{uu}n}(\mathbf{u}^n, \mathbf{u}^{n+1}, n^m) + V_{\mathbf{u}\Pi}(\mathbf{u}^{n+1}) + V_{\mathbf{u}\sigma}(\mathbf{u}^{n+1})] - \theta^2 \delta t^2 \mathcal{L}(\mathbf{u}^{n+1}) \\ &\quad = V_{\mathbf{u}n}(\mathbf{u}^n, n^m) + (1-2\theta)\delta t\, V_{\mathbf{uu}n}(\mathbf{u}^n, \mathbf{u}^n, n^m) + (1-\theta)\delta t[V_{\mathbf{u}\Pi}(\mathbf{u}^n) + V_{\mathbf{u}\sigma}(\mathbf{u}^n)] \\ &\qquad + \delta t\big[V_{\mathbf{BB}}(\mathbf{B}^m, \mathbf{B}^m) + V_p(p^m) + V_{n\mathbf{g}}(n^m)\big] - \alpha\,\delta t^2 \mathcal{L}(\mathbf{u}^n). \end{aligned} \tag{21}$$

$$\begin{aligned} &V_{\mathbf{u}n}(\mathbf{u}, n) = n\mathbf{u} \\ &V_{\mathbf{uu}n}(\mathbf{u}, \mathbf{u}, n) = -n\mathbf{u} \cdot \nabla \mathbf{u} \\ &V_{\mathbf{u}\Pi}(\mathbf{u}) = -\nabla \cdot \Pi(\mathbf{u}) \\ &V_{\mathbf{u}\sigma}(\mathbf{u}) = -\sigma \mathbf{u} \\ &V_{\mathbf{BB}}(\mathbf{B}, \mathbf{B}) = (\nabla \times \mathbf{B}) \times \mathbf{B} \\ &V_p(p) = -\nabla p \\ &V_{n\mathbf{g}}(n) = n\mathbf{g} \end{aligned} \tag{22}$$

Here, $\mathcal{L}$ is the linear ideal MHD operator:

$$\mathcal{L}(\mathbf{u}) = [\nabla \times \nabla \times (\mathbf{u} \times \mathbf{B})] \times \mathbf{B} + (\nabla \times \mathbf{B}) \times [\nabla \times (\mathbf{u} \times \mathbf{B})] + \nabla(\mathbf{u} \cdot \nabla p + \Gamma p \nabla \cdot \mathbf{u}) - \nabla \cdot (n\mathbf{u})\mathbf{g}. \tag{23}$$

Derivation of Eq. (21) as described above obtains $\alpha = \theta(\theta - 1)$. For the moment, however, we leave the value of $\alpha$ unspecified. Also, we have allowed pressure, density, and magnetic field quantities to be specified at a different time index $(m)$ than the velocity $(n)$. Appropriate choices for $m, n$, and $\alpha$ are discussed in Section 3.2.1.

Once the advanced-time velocity has been calculated, an implicit equation for the advanced-time density independent of the advanced-time pressure and magnetic field can be solved. In this and subsequent equations, we introduce a new centering parameter, $\phi$, that will be used only for the occurrences of $\mathbf{u}$ in these equations. Taking the $\theta$-advanced $n$ and and the $\phi$-advanced $\mathbf{u}$ in the density equation, dropping terms of order $\delta t^2$, and discretizing, yields:

$$\begin{aligned} &N_n(n^{m+1}) - \theta\,\delta t\left[N_{n\mathbf{u}}(n^{m+1},\mathbf{u}^n) + N_{nD_n}(n^{m+1})\right] - \phi\,\delta t\,N_{n\mathbf{u}}(n^m,\mathbf{u}^{n+1}) \\ &\quad = N_n(n^m) + (1-\theta-\phi)\delta t\,N_{n\mathbf{u}}(n^m,\mathbf{u}^n) + (1-\theta)\delta t\,N_{nD_n}(n^m) + \delta t\,N_\sigma \end{aligned} \tag{24}$$

$$\begin{aligned} &N_n(n) = n \\ &N_{n\mathbf{u}}(n,\mathbf{u}) = -\nabla\cdot(n\mathbf{u}) \\ &N_\sigma = \sigma \\ &N_{nD_n}(n) = \nabla\cdot(D_n\nabla n) \end{aligned} \tag{25}$$

Similarly, the pressure advance is found by taking the $\theta$-advanced $p$ and $\phi$-advanced $\mathbf{u}$, and discretizing:

$$\begin{aligned} &P_p(p^{m+1}) - \theta\,\delta t[P_{p\mathbf{u}}(p^{m+1},\mathbf{u}^n) + P_{p\kappa}(p^{m+1})] - \phi\,\delta t[P_{p\mathbf{u}}(p^m,\mathbf{u}^{n+1}) + P_{\mathbf{uu}\sigma}(\mathbf{u}^{n+1},\mathbf{u}^n) + P_{\mathbf{uu}\sigma}(\mathbf{u}^n,\mathbf{u}^{n+1})] \\ &\quad = P_p(p^m) + (1-\theta-\phi)\delta t\,P_{p\mathbf{u}}(p^m,\mathbf{u}^n) + (1-2\phi)\delta t\,P_{\mathbf{uu}\sigma}(\mathbf{u}^n,\mathbf{u}^n) + (1-\theta)\delta t\,P_{p\kappa}(p^m) \\ &\qquad + \delta t\left[P_{p_e\mathbf{B}}(p_e^m,\mathbf{B}^m) + P_{\mathbf{BB}\eta}(\mathbf{B}^m,\mathbf{B}^m) + P_{\mathbf{B}\Pi_e}(\mathbf{B}^m) + P_{\mathbf{u}\Pi}(\mathbf{u}^n)\right] \end{aligned} \tag{26}$$

$$\begin{aligned} &P_p(p) = p \\ &P_{p\mathbf{u}}(p,\mathbf{u}) = -\mathbf{u}\cdot\nabla p - \Gamma p\nabla\cdot\mathbf{u} \\ &P_{p_e\mathbf{B}}(p_e,\mathbf{B}) = d_i\left[\frac{1}{n}\nabla p_e + \Gamma p_e\nabla\frac{1}{n}\right]\cdot\nabla\times\mathbf{B} \\ &P_{\mathbf{BB}\eta}(\mathbf{B},\mathbf{B}) = \eta(\nabla\times\mathbf{B})\cdot(\nabla\times\mathbf{B}) \\ &P_{\mathbf{B}\Pi_e}(\mathbf{B}) = (\Gamma-1)d_i\Pi_e : \nabla\left(\frac{1}{n}\nabla\times\mathbf{B}\right) \\ &P_{p\kappa}(p,n) = (\Gamma-1)\nabla\cdot\left[\left(\kappa_\circ + \kappa_\wedge\mathbf{b}\times + \kappa_\parallel\mathbf{bb}\cdot\right)\nabla\left(\frac{p}{n}\right)\right] \\ &P_{\mathbf{uu}\sigma}(\mathbf{u},\mathbf{u}) = \frac{1}{2}(\Gamma-1)\sigma\mathbf{u}\cdot\mathbf{u} \\ &P_{\mathbf{u}\Pi}(\mathbf{u}) = -(\Gamma-1)\Pi : \nabla\mathbf{u} \end{aligned} \tag{27}$$

Note that for this advance, $\mathbf{B}$, $p_e$, and $n$ appear but are not evaluated at the $\theta$-advanced time. This allows the pressure to be advanced independently after the velocity advance, at the expense of some terms (electron convection, $P_{p_e\mathbf{B}}$, and ohmic heating, $P_{\mathbf{BB}\eta}$), not being treated implicitly. The viscous- and electron-viscous heating terms ($P_{\mathbf{u}\Pi}$ and $P_{\mathbf{B}\Pi_e}$) are treated explicitly because they contain spatial derivatives of higher than fourth order in the flux/potential representation (these terms are extremely small when physically relevant parameters are used, so this explicit treatment does not adversely affect numerical stability).

The electron pressure and magnetic field advance equations are finally calculated together using the $\theta$-advanced $\mathbf{B}$ and $p_e$ and the $\phi$-advanced $\mathbf{u}$. In contrast to the total pressure equations, the electron pressure equation is not solved independently in order to ensure that the kinetic Alfvén wave (arising from the $\nabla p_e$ term in Eq. (7)) is treated implicitly.

$$\begin{aligned} &P_p(p_e^{m+1}) - \theta\,\delta t\Big[P_{p\mathbf{u}}(p_e^{m+1},\mathbf{u}^n) + P_{p\kappa}(p_e^{m+1}) + P_{\mathbf{BB}\eta}(\mathbf{B}^{m+1},\mathbf{B}^m) + P_{\mathbf{BB}\eta}(\mathbf{B}^m,\mathbf{B}^{m+1}) + P_{p_e\mathbf{B}}(p_e^{m+1},\mathbf{B}^m) + P_{p_e\mathbf{B}}(p_e^m,\mathbf{B}^{m+1})\Big] \\ &\quad - \phi\,\delta t P_{p\mathbf{u}}(p_e^m,\mathbf{u}^{n+1}) = P_p(p_e^m) + (1-\theta-\phi)\delta t\,P_{p\mathbf{u}}(p_e^m,\mathbf{u}^n) + (1-2\theta)\delta t\left[P_{\mathbf{BB}\eta}(\mathbf{B}^m,\mathbf{B}^m) + P_{p_e\mathbf{B}}(p_e^m,\mathbf{B}^m)\right] \\ &\quad + (1-\theta)\delta t\,P_{p\kappa}(p_e^m) + \delta t\,P_{\mathbf{B}\Pi_e}(\mathbf{B}^m) \end{aligned} \tag{28}$$

$$\begin{aligned} &B_{\mathbf{B}}(\mathbf{B}^{m+1}) - \theta\,\delta t\Big[B_{\mathbf{Bu}}(\mathbf{B}^{m+1},\mathbf{u}^n) + B_{\mathbf{B}\eta}(\mathbf{B}^{m+1}) + B_{\mathbf{BB}}(\mathbf{B}^{m+1},\mathbf{B}^m) + B_{\mathbf{BB}}(\mathbf{B}^m,\mathbf{B}^{m+1}) + B_{p_e}(p_e^{m+1}) + B_{\mathbf{B}\Pi_e}(\mathbf{B}^{m+1})\Big] \\ &\quad - \phi\,\delta t\,B_{\mathbf{Bu}}(\mathbf{B}^m,\mathbf{u}^{n+1}) = B_{\mathbf{B}}(\mathbf{B}^m) + (1-\theta-\phi)\delta t\,B_{\mathbf{Bu}}(\mathbf{B}^m,\mathbf{u}^n) \\ &\quad + (1-2\theta)\delta t\,B_{\mathbf{BB}}(\mathbf{B}^m,\mathbf{B}^m) + (1-\theta)\delta t[B_{\mathbf{B}\eta}(\mathbf{B}^m) + B_{p_e}(p_e^m) + B_{\mathbf{B}\Pi_e}(\mathbf{B}^m)] \end{aligned} \tag{29}$$

$$\begin{aligned} &B_{\mathbf{B}}(\mathbf{B}) = \mathbf{B} \\ &B_{\mathbf{Bu}}(\mathbf{B},\mathbf{u}) = \nabla\times(\mathbf{u}\times\mathbf{B}) \\ &B_{\mathbf{B}\eta}(\mathbf{B}) = -\nabla\times(\eta\nabla\times\mathbf{B}) \\ &B_{\mathbf{BB}}(\mathbf{B},\mathbf{B}) = -d_i\nabla\times\left[\frac{1}{n}(\nabla\times\mathbf{B})\times\mathbf{B}\right] \\ &B_{p_e}(p_e) = d_i\nabla\times\left(\frac{1}{n}\nabla p_e\right) \\ &B_{\mathbf{B}\Pi_e}(\mathbf{B}) = d_i\nabla\times\left[\frac{1}{n}\nabla\cdot\Pi_e(\mathbf{B})\right] \end{aligned} \tag{30}$$

*3.2.1. Comparison of time step methods*

We now return to the issue of appropriate choices for $m, n, \phi$, and $\alpha$. One choice which leads to a meaningful algorithm is $m = n, \phi = \theta$, and $\alpha = \theta(\theta - 1)$, to which we will refer as the split $\theta$-implicit timestep. The further choice $\theta = \frac{1}{2}$ could be called the split Crank–Nicholson timestep, and is accurate to second order in $\delta t$ (see Appendix B).

Caramana has shown that the choice $\alpha = \theta^2$ leads to a stable method with less numerical dissipation than with $\alpha = \theta(\theta - 1)$ [30,23]. Furthermore, this timestep is accurate to second order in $\delta t$ for any stable value of $\theta$ when $\phi = 1$ and $m = n + \frac{1}{2}$ (i.e. leapfrog). We will refer to this method as the "Caramana method." A significant advantage of this method for our purposes is that stationary solutions of the Caramana discretization are much more accurate than those of the split $\theta$-implicit discretization when $\delta t$ is large. Heuristically, this can be seen by observing that the $\mathcal{L}$ terms cancel in the stationary solution of Eq. (21) only when $\alpha = \theta^2$, if $\mathcal{L}(\mathbf{u}) \neq 0$ (which is true except in the static, ideal limit). A detailed analysis of the stability, truncation error, and stationary solution accuracy of the Caramana method is presented in Appendix B.

Finally, an "unsplit" method may be constructed simply by taking Eqs. (24), (26), (28), and (29) together with a momentum equation derived in the same way as the field equations (i.e. without the parabolization) into a single matrix equation. For the unsplit advance, the choice $m = n$ and $\phi = \theta$ yields the unsplit $\theta$-implicit method, or the Crank–Nicholson method when $\phi = \theta = \frac{1}{2}$. The unsplit method is significantly less efficient than the split methods, and is implemented primarily for diagnostic purposes. It requires the solution of a single ill-conditioned rank $8N$ matrix equation, as opposed to the split methods, which require the solution of two rank $3N$ and two rank $N$ matrix equations, each of which are relatively well-conditioned [29].

Fig. 2 shows a comparison of the steady-state kinetic energy between the Caramana method, the split $\theta$-implicit method, and the unsplit method. The unsplit method is found to be the most accurate, but the Caramana method gives relatively accurate results at significantly lower computational cost (for a given value of $\delta t$).

*3.2.2. Iteration of magnetic field advance*

It is empirically found that, for low values of resistivity, when ohmic heating, strongly anisotropic thermal conductivity, and flow are included, the split method described above may become unstable at unacceptably small values of $\delta t$. This limitation has been overcome by implementing a predictor-corrector scheme in which after the time step is completed, the transport coefficients ($\eta$ in particular) are calculated, and then the magnetic field/pressure advance is re-calculated using the new values of the transport coefficients. This iteration has no effect on the steady-state solution. A single iteration of this type increases the computational cost of a time step by roughly 50%, but may improve the maximum stable time step by several orders of magnitude. Fig. 3 shows that the iteration method raises the maximum value of $\delta t/\tau_{A0}$ from $\mathcal{O}(10^{-2})$ to $\mathcal{O}(1)$, for a typical case ($\eta_0 = 10^{-4}$). (see Fig. 4)

*3.2.3. Scalar representation*

Eqs. (21), (24), (26), (28), and (29) constitute the discretized equations to be solved each time advance. To solve these equations, a coordinate system and scalar representation for $\mathbf{B}$ and $\mathbf{u}$ must be chosen. We use cylindrical coordinates $(R, \varphi, Z)$ (where $\varphi$ is the ignorable coordinate in the two-dimensional simulations presented here) and the flux/potential representation of the magnetic and velocity fields,

$$\mathbf{B} = \nabla\psi \times \nabla\varphi + I\nabla\varphi \tag{31}$$

$$\mathbf{u} = \nabla U \times \nabla\varphi + V\nabla\varphi + \nabla\chi. \tag{32}$$

(The scalar equations are also implemented in Cartesian coordinates $(x, y, z)$, with $\varphi \rightarrow y$ in Eqs. (31) and (32); however, only applications using cylindrical coordinates are discussed here.) This representation has several advantages. First, the magnetic field is completely determined by the values of only two fields, $\psi$ and $I$, and the condition $\nabla \cdot \mathbf{B} = 0$ is always exactly satisfied. Second, the solenoidal, toroidal, and compressible parts of the velocity are naturally separated. Third, there

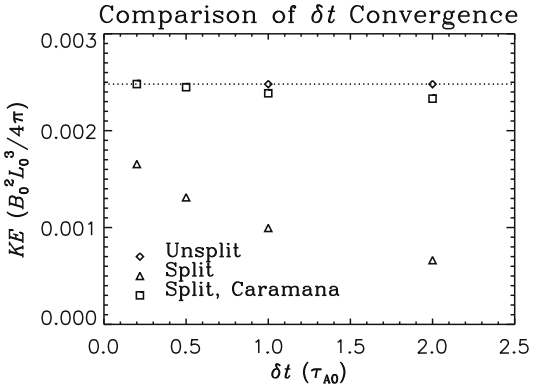


**Fig. 2.** The stationary steady-state kinetic energy is plotted as a function of timestep $\delta t$ for simulations run with different time-stepping methods: the Caramana method, the split $\theta$-implicit method, and the unsplit $\theta$-implicit method.

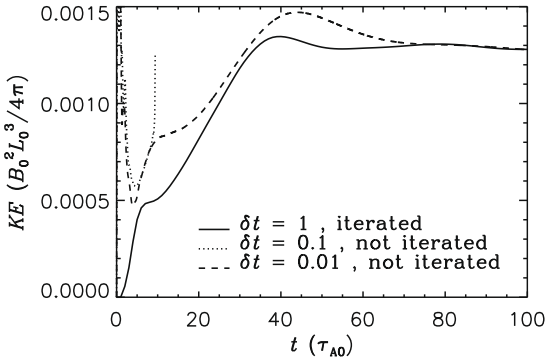


**Fig. 3.** The time evolution of the kinetic energy for various values of $\delta t$. In this case, the method without iterating the field-solve is stable for $\delta t = 0.01\tau_{A0}$, but not for $\delta t = 0.1\tau_{A0}$. When the field-solve iteration is used, $\delta t = \tau_{A0}$ is stable.

exist two subsets of the full system of equations which are easily recovered using this representation: one is the "two-field" equations of reduced MHD which are recovered by evolving only $\psi$ and $U$; the other is the "four-field" equations of Fitzpatrick [31] which are recovered by evolving only $\psi, U, I$, and $V$. It can be shown that each of these subsets is self-consistent and conserves energy (excluding dissipative terms).

The main disadvantage of the flux/potential formulation is that it requires more spatial derivatives than would simply breaking **B** and **u** into their spatial coordinate components. Use of $C^1$ elements eliminates this concern, as almost no physical term has more than four spatial derivatives using the flux/potential representation, and therefore no auxiliary variables need be defined.[1]

Each equation must be broken into scalar components, and cast in the weak form necessary for computation using finite elements. This is done by acting on the vector equations with various projection operators (see Appendix C). The end result of this process is a set of equations which can be written in the following block-matrix form:

$$\begin{pmatrix} S_{UU} & S_{UV} & S_{U\chi} \\ S_{VU} & S_{VV} & S_{V\chi} \\ S_{\chi U} & S_{\chi V} & S_{\chi\chi} \end{pmatrix} \begin{pmatrix} U \\ V \\ \chi \end{pmatrix}^{n+1} = \begin{pmatrix} D_{UU} & D_{UV} & D_{U\chi} \\ D_{VU} & D_{VV} & D_{V\chi} \\ D_{\chi U} & D_{\chi V} & D_{\chi\chi} \end{pmatrix} \begin{pmatrix} U \\ V \\ \chi \end{pmatrix}^{n} + \begin{pmatrix} Q_{U\psi} & Q_{UI} & Q_{Up} & Q_{Un} \\ Q_{V\psi} & Q_{VI} & Q_{Vp} & Q_{Vn} \\ Q_{\chi\psi} & Q_{\chi I} & Q_{\chi p} & Q_{\chi n} \end{pmatrix} \begin{pmatrix} \psi \\ I \\ p \\ n \end{pmatrix}^{m} + \begin{pmatrix} O_U \\ O_V \\ O_\chi \end{pmatrix} \tag{33}$$

$$S_{nn} n^{m+1} = D_{nn} n^m + \begin{pmatrix} R_{nU} & R_{nV} & R_{n\chi} \end{pmatrix} \begin{pmatrix} U \\ V \\ \chi \end{pmatrix}^{n+1} + \begin{pmatrix} Q_{nU} & Q_{nV} & Q_{n\chi} \end{pmatrix} \begin{pmatrix} U \\ V \\ \chi \end{pmatrix}^{n} + O_n \tag{34}$$

$$S_{pp} p^{m+1} = D_{pp} p^m + \begin{pmatrix} R_{pU} & R_{pV} & R_{p\chi} \end{pmatrix} \begin{pmatrix} U \\ V \\ \chi \end{pmatrix}^{n+1} + \begin{pmatrix} Q_{pU} & Q_{pV} & Q_{p\chi} \end{pmatrix} \begin{pmatrix} U \\ V \\ \chi \end{pmatrix}^{n} + O_p \tag{35}$$

$$\begin{pmatrix} S_{\psi\psi} & S_{\psi I} & S_{\psi p_e} \\ S_{I\psi} & S_{II} & S_{Ip_e} \\ S_{p_e\psi} & S_{p_eI} & S_{p_ep_e} \end{pmatrix} \begin{pmatrix} \psi \\ I \\ p_e \end{pmatrix}^{m+1} = \begin{pmatrix} D_{\psi\psi} & D_{\psi I} & D_{\psi p_e} \\ D_{I\psi} & D_{II} & D_{Ip_e} \\ D_{p_e\psi} & D_{p_eI} & D_{p_ep_e} \end{pmatrix} \begin{pmatrix} \psi \\ I \\ p_e \end{pmatrix}^{m} + \begin{pmatrix} R_{\psi U} & R_{\psi V} & R_{\psi\chi} \\ R_{IU} & R_{IV} & R_{I\chi} \\ R_{p_eU} & R_{p_eV} & R_{p_e\chi} \end{pmatrix} \begin{pmatrix} U \\ V \\ \chi \end{pmatrix}^{n+1} + \begin{pmatrix} Q_{\psi U} & Q_{\psi V} & Q_{\psi\chi} \\ Q_{IU} & Q_{IV} & Q_{I\chi} \\ Q_{p_eU} & Q_{p_eV} & Q_{p_e\chi} \end{pmatrix} \begin{pmatrix} U \\ V \\ \chi \end{pmatrix}^{n} + \begin{pmatrix} O_\psi \\ O_I \\ O_{p_e} \end{pmatrix}. \tag{36}$$

The elements of these matrices are each linear operators defined in Appendix C. The two-field or four-field reduced MHD equations may be obtained simply by taking the upper-left $1 \times 1$ or $2 \times 2$ sub-matrices of the S, D, R, and Q matrices above.

In the present work for simplicity we focus on the case where only the total pressure is evolved, and the ion and electron pressures are held as fixed fractions of the total pressure. This is done by excluding Eq. (35) from the time-step, and replacing the electron pressure equation with the total pressure equation in Eq. (36).

## 4. Axisymmetric steady-states

We have used M3D-$C^1$ to calculate the axisymmetric steady-states of Eqs. (1)–(5) in a toroidal, NSTX-like configuration using the following method. The initial conditions for the pressure and magnetic field are determined by calculating a static

[1] The viscous and electron-viscous heating terms do contain terms having more than four derivatives; however, these terms are generally small and may be treated explicitly without affecting numerical stability.

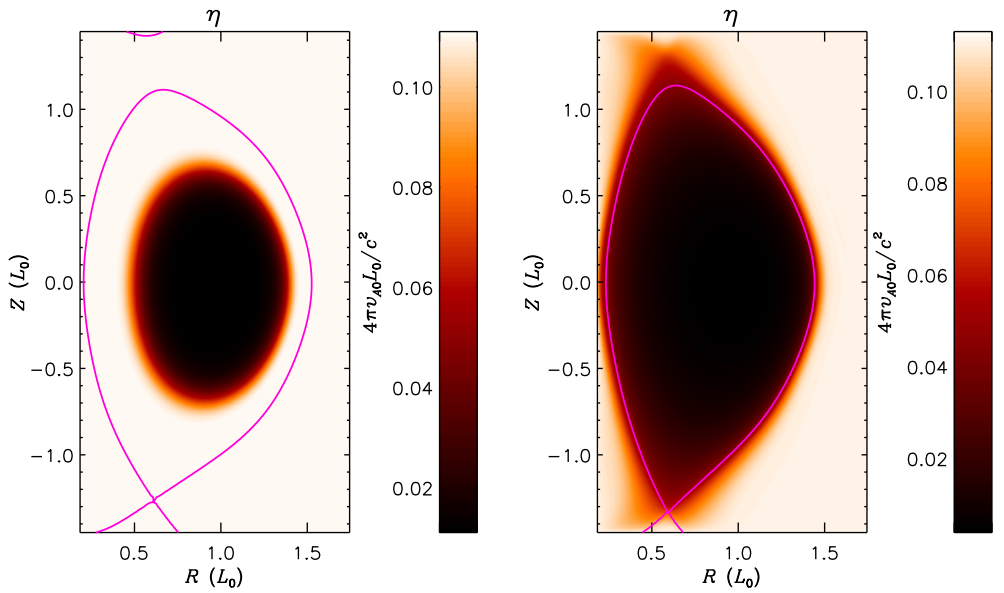


**Fig. 4.** The normalized resistivity in the initial conditions (left) and in the final steady-state (right) is shown. In both cases, $\eta$ ranges from roughly 0.1 at the edge to .004 at the magnetic axis.

ideal-MHD equilibrium subject to fields due to currents in external magnetic coils (outside the simulation domain) appropriate to NSTX. The precise method for obtaining this solution is described in detail in reference [24]. This initial condition satisfies the GS equation, $R^2\nabla\cdot(\nabla\psi/R^2) = -R^2p(\psi) - I(\psi)I'(\psi)$, and is not, in general, a stationary solution of the two-fluid equations. The initial density is taken to be a fractional power of the total pressure, $n = p^x$, typically with $x = 0.3$.

The system is then time-advanced according to the dynamical two-fluid equations. In order to counteract the resistive dissipation of current, a loop voltage $V_L$ is applied by ramping up the value of the poloidal flux $\psi$ on the boundary at a rate $\dot{\psi} = V_L/2\pi$. The loop voltage is regulated by a PID controller to keep the toroidal current at a fixed value. This loop voltage also serves to counteract the diffusion of thermal energy out of the domain by causing ohmic (Joule) heating; no other energy source is included. The thermal conductivity is chosen so that the temperature attains a realistic value in steady-state. Particle loss due to diffusive flux out of the domain is counteracted by a localized particle source $\sigma$ near the magnetic axis, on the high-field side (HFS) unless otherwise noted.

The simulation results presented here were done using a diverted magnetic configuration typical of NSTX. Resistivity was taken to be defined by Eq. (9), with results here obtained with $\eta_0$ in the range $10^{-4} - 10^{-6}$. The other transport parameters, $\kappa_\circ, \kappa_\parallel, D_n, \mu$, and $\mu_c$, were taken to be constant and uniform. Unless otherwise specified, $\kappa_\circ = 200\eta_0, \kappa_\wedge = 0, \kappa_\parallel/\kappa_\circ = 10^4, D_n = 10^{-4}, \mu = 10^{-4}$, and $\mu_c = 10^{-3}$. ($\kappa$ is scaled with resistivity in order to achieve temperature profiles roughly independent of $\eta_0$). For two-fluid simulations, the ion skin depth was a realistic value of $d_i = 5.1\times10^{-2}$. One-fluid simulations were done by letting $d_i = 0$. Since the gyroviscous force scales with $d_i$, it is not included in one-fluid simulations.

The system of equations considered here are a driven, nonlinear system, and may not have a unique stationary steady-state, or any stationary state at all. However, for the cases presented below, which are carried out with relatively large values of dissipation, the system is typically found to relax to a steady-state within 5-10 resistive periods ($\eta^{-1}$). These states are steady on all time-scales present in the model, including hydrodynamic, diffusive, and resistive scales. It is found that simulations obtain the same steady-state whether the initial conditions are an ideal MHD equilibrium (as described above), or a resistive one-fluid equilibrium with flow (which itself may be obtained by M3D-$C^1$ using a reduced model). This does not prove that the steady-states found here are unique in a global sense, but it is evidence that the steady-states are not invariant to continuous transformations of any quantity, as is the case in dissipationless models (i.e. there are no "free functions" whose values are continuous functions of the initial conditions).

Some simulations using smaller values of resistivity ($\eta_0 \lesssim 10^{-5}$) and viscosity ($\mu \lesssim 10^{-5}$) are found not to approach a stationary steady-state, but remain oscillatory on time-scales long compared to any individual dissipative time-scales in the system. Even in these oscillatory cases, the magnitude of the persistent fluctuations is small relative to the main features of the mean steady-state profiles. The following discussion focuses mainly on cases in which a stationary state is indeed reached. The theory of the transition from stationary to non-stationary steady-states is not considered here.

In these simulations, between 3200 and 4382 reduced quintic elements were typically used. Some cases were tested for spatial convergence using up to 12800 elements. In one such case, in which the steady-state is essentially stationary ($\eta_0 = 10^{-5}$), it is found that quadrupling the number of elements from 3200 to 12,800 (i.e. halving the linear scale of the elements) results in a 9% change in the total kinetic energy. Most of this change is due to flows at plasma-vacuum boundary,

especially on the high-field side where the plasma-vacuum boundary comes very close to the simulation domain boundary, which are evidently not fully resolved in the lower-resolution case. However, this difference is only quantitative in nature; the qualitative flow patterns are unaffected.

### 4.1. Thermodynamic profiles

Eqs. (1), (2), (4), and (5) may be combined to yield the equation of energy conservation

$$\frac{\partial}{\partial t}\left[B^2+\frac{1}{2}nu^2+\frac{p}{\Gamma-1}\right]+\nabla\cdot\left[\frac{\Gamma}{\Gamma-1}\left(p\mathbf{u}-\frac{d_i}{n}p_e\mathbf{J}\right)+\frac{1}{2}nu^2\mathbf{u}+\mathbf{E}\times\mathbf{B}+\Pi\cdot\mathbf{u}-\frac{d_i}{n}\Pi_e\cdot\mathbf{J}+\mathbf{q}\right]=n\mathbf{g}\cdot\mathbf{u}. \tag{37}$$

In a stationary steady-state and in the absence of external sources (i.e. gravity), the fluxes (terms within the divergence) must balance. In Eq. (37), these terms respectively represent the pressure (thermal energy) convection, kinetic energy convection, Poynting flux, ion and electron-viscous fluxes, and heat flux. Fig. 6 shows the result of operating on Eqs. (37) and (1), term by term, with $A^{-1}\int_V dV$, where $V$ is the volume enclosed by each magnetic surface, and $A$ is the area of that surface, for a two-fluid steady-state with $\eta_0 = 10^{-5}$. For the parameters investigated here, the energy balance within the last closed flux surface (LCFS)—the magnetic surface farthest from the magnetic axis that does not intersect the domain boundary—is always dominated by the balance between ohmic heating and perpendicular thermal diffusive losses.

$$\frac{\eta_0}{T^{3/2}}J^2\approx\nabla\cdot(\kappa_\circ\nabla T). \tag{38}$$

Therefore, by keeping $\kappa_\circ/\eta_0$ the same for each simulation, the temperature profile is essentially the same in each, as can be seen in Fig. 5. However, the pressure and density profiles differ somewhat among simulations with varying $\eta_0$. Due to the increased Pfirsch-Schlüter convective losses at higher resistivity (see Section 4.2), the core density (and hence pressure) is higher in the low-resistivity cases. The safety factor at the magnetic axis is slightly lower in the low-resistivity cases, with $q_0\approx 0.9$ in the $\eta_0 = 10^{-4}$ case and $q_0\approx 0.8$ at $\eta_0 = 10^{-6}$. (The safety factor is a property of magnetic surfaces, and is defined as the number of toroidal transits made by a magnetic field line as it completes a single poloidal transit on the surface.) Two-fluid terms and gyroviscosity are entirely negligible in the particle, radial momentum, and energy balances, and do not directly contribute to cross-field fluxes; therefore the thermodynamic and magnetic profiles are not sensitive to the inclusion of these effects.

The radial electric field, shown in Fig. 7, is found to be negative (inward) throughout the plasma. This is due primarily to the relatively large ion pressure gradient. In experiments with auxiliary methods of heating (other than ohmic heating) operating in H-mode, it is found that the radial electric field exhibits a dramatic drop at the edge concurrent with the formation of sharp temperature and density gradients. The thermodynamic profiles in the simulation results presented here lack such sharp gradients, and more closely resemble L-mode profiles characteristic of ohmic discharges.

### 4.2. Radial flows

It is well known that resistive diffusion in a toroidal magnetic configuration leads to parallel currents and cross-field convective transport [32]. The radial flows responsible for this transport may be derived from the resistive Ohm's law, assuming ideal force balance and $\nabla\cdot\mathbf{J}=0$, to be

$$\mathbf{u}\cdot\nabla\psi=-\frac{V_L}{2\pi}\left(1-\frac{\langle B_\varphi^2\rangle}{\langle B^2\rangle}\right)-\eta p' R^2\left(1-\frac{B_\varphi^2}{\langle B^2\rangle}\right). \tag{39}$$

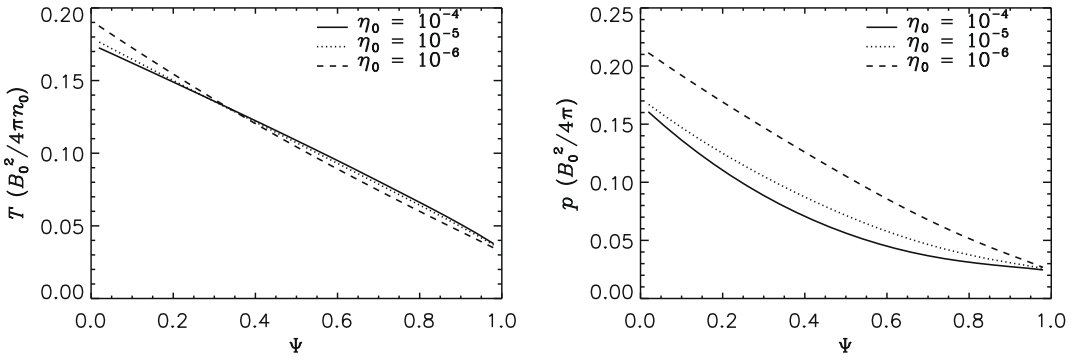


**Fig. 5.** The surface-averaged steady-state temperature (left) and pressure (right) profiles as a function of normalized flux $\Psi$. The magnetic axis is $\Psi = 0$, and the LCFS is $\Psi = 1$.

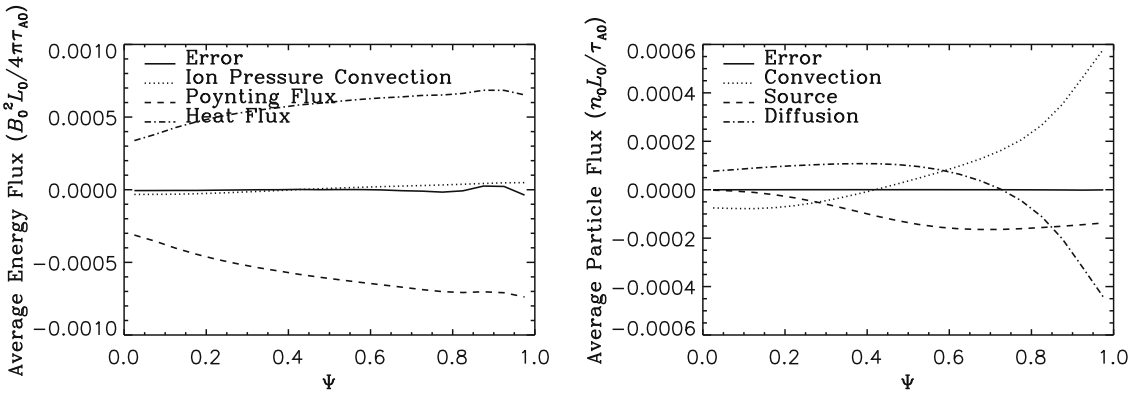


**Fig. 6.** The surface-averaged energy balance (left) and particle balance (right) in the steady-state of a two-fluid simulation with $\eta_0 = 10^{-5}$. Positive values indicate outward flux. Smaller terms in the energy balance such as electron pressure convection, kinetic energy convection, and viscous fluxes are suppressed. The Poynting flux is $V_L I_p$, where $V_L$ is the loop voltage and $I_p$ is the plasma current, and represents the energy transferred to the plasma by ohmic heating.

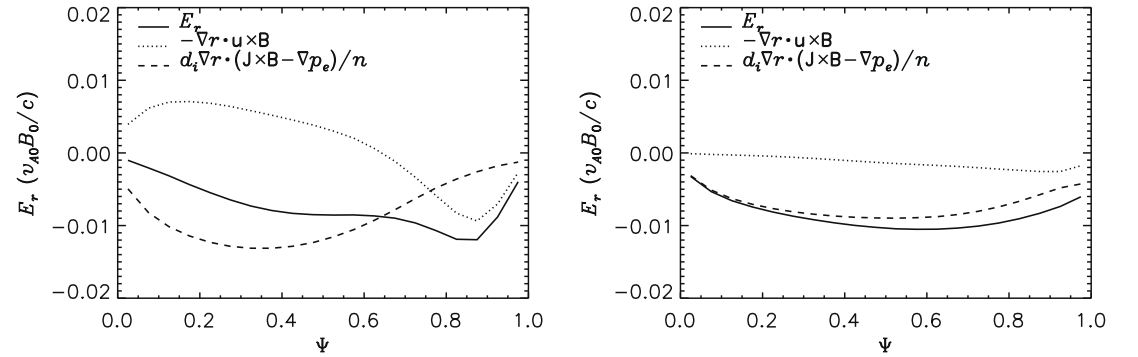


**Fig. 7.** The surface-averaged radial electric field in the steady-state with $\eta_0 = 10^{-4}$ (left) and $\eta_0 = 10^{-5}$ (right), as calculated from Eq. (7). The quantity $d_i \hat{\mathbf{r}} \cdot (\mathbf{J} \times \mathbf{B} - \nabla p_e)/n$ is equivalent to $d_i \hat{\mathbf{r}} \cdot \nabla p_i/n$ up to small inertial and viscous effects. Here $\hat{\mathbf{r}} = -\nabla\psi/|\psi|$ is the outward minor-radial direction.

Here, $\langle a \rangle = \oint (a\, dl/|B_p|)/\oint (dl/|B_p|)$ is the magnetic surface average, where $|B_p| = |\mathbf{B} - B_\varphi R \nabla\varphi|$ is the poloidal field strength, $B_\varphi = R\mathbf{B} \cdot \nabla\varphi$ is the toroidal field strength, and $dl$ is a differential arc-length tangent to the poloidal field. In Fig. 8, the left and right sides of Eq. (39), as calculated from several computed stead-states, are compared. For the cases which reach a stationary steady-state, Eq. (39) is found to be well satisfied, with some discrepancy near the LCFS where stronger poloidal variations in pressure begin to occur. The $\eta_0 = 10^{-6}$ case remains oscillatory in the core in the two-fluid model, and there is some deviation from Eq. (39) in that case.

### 4.3. Toroidal flows

It was previously found in simulations using a resistive one-fluid model [3] that the toroidal flows in the resistive scrape-off layer (SOL)—the region immediately outside the LCFS—are dominantly up-down antisymmetric. Furthermore, these flows were found to be quite strong—of order 100 km/s—when the Lundquist number of the SOL is of order 10. We find results similar in both character and magnitude in cases where the SOL Lundquist number is comparable; however, the situation changes at lower resistivities.

The steady-state toroidal flow patterns in a series of our simulations are shown in Fig. 9. The dominant feature of the high-resistivity cases is the nearly up-down antisymmetric edge flow. As resistivity is uniformly decreased, the strength of this edge flow decreases, and is dominated by an up-down symmetric toroidal flow in the core when $\eta_0 = 10^{-6}$. (Though there exist small oscillations in this particular steady-state, this toroidal rotation feature is persistent and essentially stationary.) This toroidal flow is due to a combination of gyroviscosity and the particle source. Specifically, the region of increased density at the position of the particle source leads to divergent flows away from the source, primarily aligned with the magnetic field. There is a vertical gradient in the toroidal component of this field-aligned flow, which leads to a toroidal gyroviscous force. This process is described in more detail in Ref. [33]. By relocating the particle source from the HFS to the LFS, the direction of this toroidal rotation is reversed. This effect becomes more evident at lower resistivity, when the resistively driven flows are smaller.

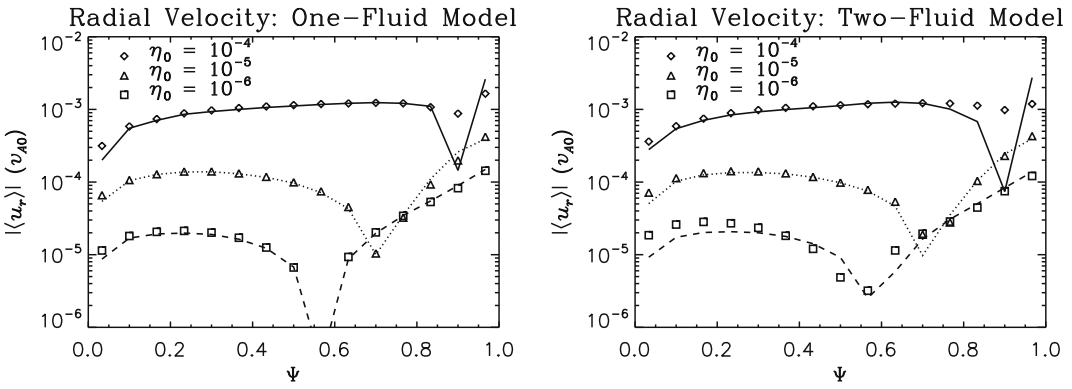


**Fig. 8.** The surface-averaged value of $u_r = -\mathbf{u} \cdot \nabla\psi/|\nabla\psi|$ is plotted versus normalized flux ($\Psi = 0$ at the magnetic axis, $\Psi = 1$ at the LCFS), for various values of $\eta_0$. Left: one-fluid simulations; right: two-fluid simulations (including gyroviscosity). Symbols indicate actual velocity values from the simulations, and lines represent the expected values according to Eq. (39). The minimum in each line represents the point at which the sign of $\langle u_r \rangle$ changes from inward (toward the magnetic axis) to outward (toward the LCFS).

Another significant and unexpected effect of gyroviscosity is a highly regular oscillation which is found to occur in high-resistivity cases ($\eta_0 \gtrsim 10^{-4}$). This oscillation is damped by isotropic viscosity, and may persist for long periods when the isotropic viscosity is relatively small (see Fig. 10). The amplitude appears to be independent of the initial conditions, which suggests that the oscillation is nonlinear in nature. The frequency and amplitude of this oscillation are independent of the numerical parameters $\delta t$ and $\delta x$; furthermore, the "eigenfunction" of the oscillation (approximated by taking the difference of the scalar fields at the peak and trough of the oscillation) does not exhibit any sharp features, nor is it localized near the boundaries of the simulation domain. Though we are confident that these oscillations arise from the dynamical equations of our model and are not numerical in nature, neither it is clear that they are physical, as they may be affected by corrections to the gyroviscosity not present in the Braginskii form [34].

Neither the core toroidal rotation nor the steady oscillation phenomenon are present in the absence of gyroviscosity, in which case the toroidal flow in the core is found to be very weak and essentially up-down antisymmetric throughout (i.e. no net toroidal flow in the core). A detailed analysis of toroidal flows in the presence of gyroviscosity and local particle sources will be presented in a future publication.

For the simulation parameters in this study, isotropic viscosity plays an important role in the magnitude of the toroidal flows and the character of the steady-state. An analysis of simulation results shows that the dominant terms in the local toroidal angular momentum balance changes as viscosity is decreased. For the $\eta_0 = 10^{-4}$ cases without gyroviscosity or parallel viscosity, the balance is between the $\mathbf{J} \times \mathbf{B}$ torque and the viscosity when $\mu \gtrsim 10^{-4}$; when $\mu \lesssim 10^{-4}$, the balance is dominantly between the $\mathbf{J} \times \mathbf{B}$ torque and convection. In the higher-viscosity cases, the stationary steady-states are obtained, whereas in lower-viscosity cases the kinetic energy exhibits small, persistent fluctuations in the steady-state.

### 4.4. Poloidal rotation

Vector plots of the poloidal velocity for various resistivities are shown in Fig. 11. In the high resistivity ($\eta_0 = 10^4$) case, these flows are dominated by the Pfirsch-Schlüter flows across the magnetic surfaces from the HFS to the LFS, with strong

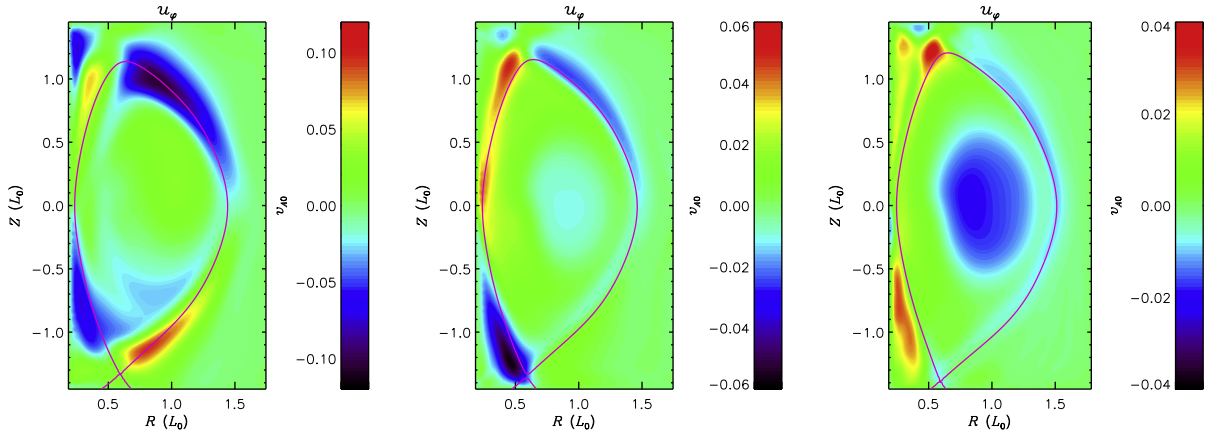


**Fig. 9.** Plots of the toroidal velocity for (from left to right) $\eta_0 = 10^{-4}, 10^{-5}$, and $10^{-6}$.

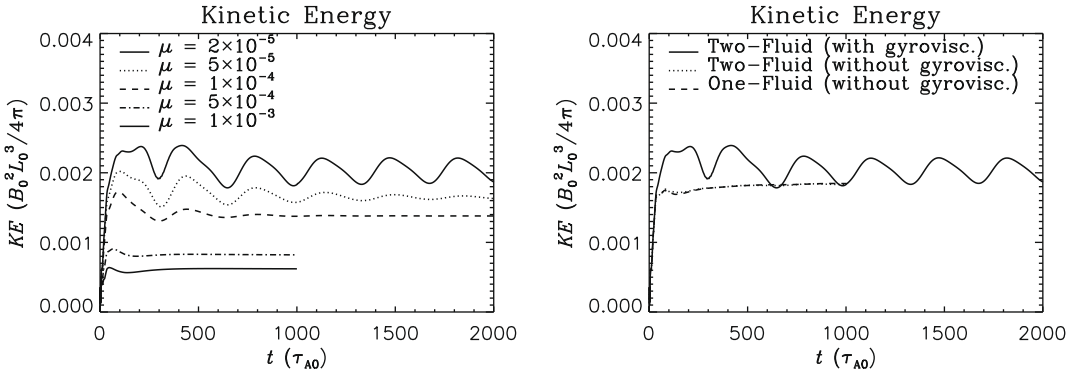


**Fig. 10.** Left: The total kinetic energy versus time for the two-fluid model, including gyroviscosity, for various values of isotropic viscosity $\mu$. Right: the total kinetic energy for various models—one-fluid (without gyroviscosity), two-fluid without gyroviscosity, and two-fluid with gyroviscosity—at $\mu = 2 \times 10^{-5}$. These results are all from simulations having $\eta_0 = 10^{-4}$.

vertical return flows along the center stack toward the horizontal mid-plane. These observations are in agreement with both the observations that fuel injection is significantly more efficient from the HFS than from the LFS, and that the injection from the HFS corners is as efficient as injection from the HFS mid-plane [35]. As resistivity is decreased, this convection pattern is no longer permitted since the cross-surface flows are proportional to the resistivity; the poloidal flows are instead dominated by a poloidal rotation in the electron diamagnetic drift direction.

When gyroviscosity is included, a new rotation near the magnetic axis becomes apparent. This is due to the toroidal gyroviscous torque described in the previous section driving a parallel flow. The simulations shown in Fig. 11 are such that the toroidal gyroviscous force is in the negative $\hat{\boldsymbol{\varphi}}$ direction. Since $B_\varphi < 0$ and $J_\varphi > 0$ in this case, the poloidal component of this flow is in the ion diamagnetic direction. In the case where the particle source is moved to the LFS, for example, this poloidal rotation would be in the electron diamagnetic direction, thereby enhancing the ambient poloidal flow. These results are obtained in the absence of parallel viscosity, which has the effect of strongly damping poloidal rotation (though not the toroidal flows), as described below.

*4.4.1. Parallel viscosity*

The collisional parallel viscous stress represents the deviation of the pressure from pure isotropy, under the assumption that this deviation is small compared to $p$. In a low-collisionality plasma ($\nu_i \ll \omega_{ci}$), the parallel viscosity is formally the largest component of the viscous stress tensor $\Pi$. Parallel viscosity contains the physical effect of magnetic pumping, the main effect of which in tokamak geometries is to damp out poloidal rotation of the plasma [36].

It can be shown that this poloidal damping in an axisymmetric toroidal system is a consequence of the minimization of the entropy production of the parallel viscosity, which is proportional to $(\mathbf{b} \cdot \mathrm{W} \cdot \mathbf{b})^2$, together with constraints on velocity profile imposed by Ohm's law [33].

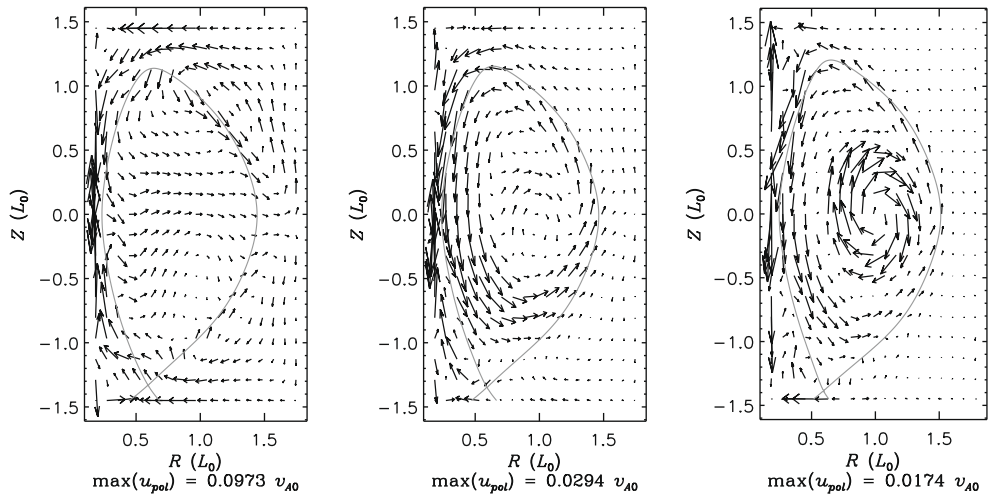


**Fig. 11.** Plots of the poloidal velocity for (from left to right) $\eta_0 = 10^{-4}, 10^{-5}$, and $10^{-6}$. In these cases, the parallel viscosity has been neglected. The core rotation is due to the toroidal gyroviscous force arising from a localized particle source driving parallel flows (see text).

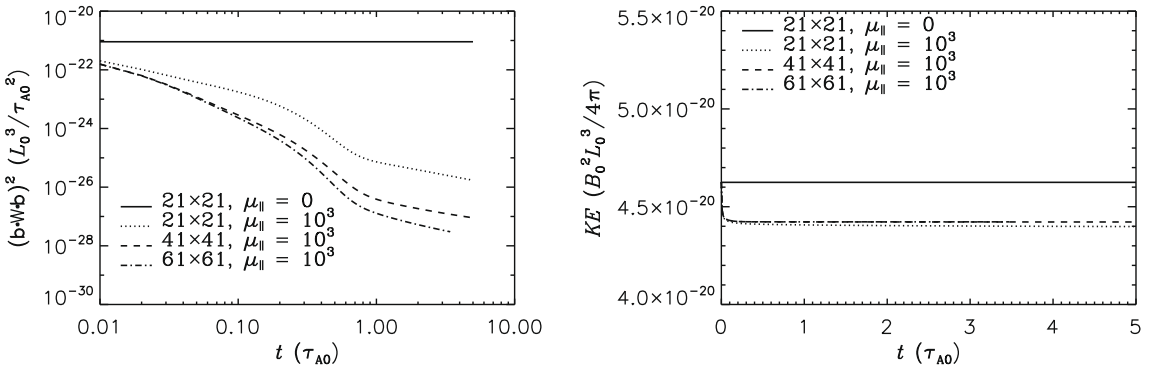


**Fig. 12.** Left: The time series of $(\mathbf{b}\cdot\mathrm{W}\cdot\mathbf{b})^2$ for a test of the linear damping of flows in NSTX geometry by parallel viscosity (see text), for various mesh resolutions. One case without parallel viscosity is shown; the others have $\mu_\parallel = 10^3$. Right: the corresponding time series of the kinetic energy.

There does not appear to be a standard method or test case for verifying the implementation of parallel viscosity, which is somewhat more complicated than parallel thermal conductivity. One effect that should be apparent in the presence of strong parallel viscosity is that the quantity $(\mathbf{b}\cdot\mathrm{W}\cdot\mathbf{b})^2$ should be minimized. To test this in controlled circumstances, we have run linear simulations, initialized in the same NSTX-like GS equilibrium as our other simulations, but given a very small initial poloidal rotation ($\sim 10^{-10} v_{A0}$). The system is then evolved keeping density, pressure, and the magnetic field constant (i.e. only the momentum equation is evolved). The results of this test are shown in Fig. 12. It is found that $(\mathbf{b}\cdot\mathrm{W}\cdot\mathbf{b})^2$ rapidly drops several orders of magnitude when parallel viscosity is included. The kinetic energy (which is due at all times almost entirely to poloidal flows) is found not to damp significantly; this is because the toroidal angular velocity is not constrained to remain constant within magnetic surfaces in the absence of Ohm's law in this test case. This demonstrates that our implementation of the parallel viscosity damps $(\mathbf{b}\cdot\mathrm{W}\cdot\mathbf{b})^2$, as it should, but not simply by damping the kinetic energy.

The effect of parallel viscosity in a nonlinear NSTX-geometry simulation using the full two-fluid model is shown in Fig. 13, in which the steady-state poloidal flow from cases with and without parallel viscosity is plotted. It can be seen that the inclusion of strong parallel viscosity has the effect of essentially eliminating the poloidal rotation, resulting in a more closely up-down symmetric flow. The dominant features of the toroidal velocity, including the toroidal flow driven by gyroviscosity in the presence of a particle source, are found to remain essentially unchanged by parallel viscosity.

## 5. Discussion and conclusions

We have developed and demonstrated a method for obtaining time-dependent solutions of a physically comprehensive, nonlinear, two-fluid plasma model, subject to initial and boundary conditions, in axisymmetric toroidal geometry. Using M3D-C[1], steady-states of this model have been obtained for NSTX-geometry plasmas by time-integration of the dynamical, driven system. Some of these states are found to be essentially stationary on all time-scales, and others

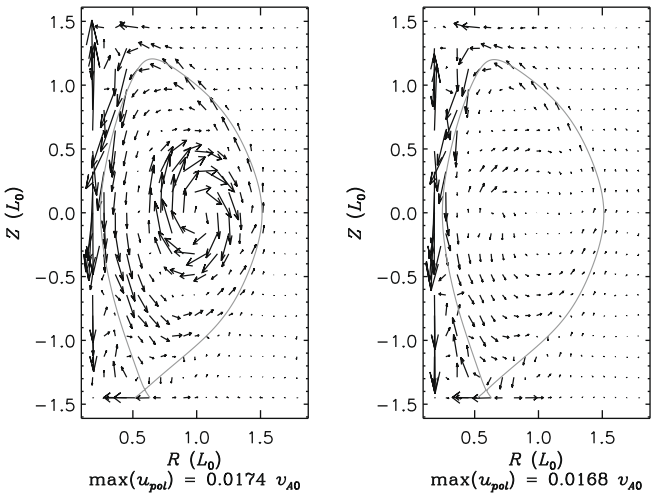


**Fig. 13.** The poloidal projection of the velocity with $\mu_\parallel = 0$ (left) and $\mu_\parallel = 10$ (right), in the case where $\eta_0 = 10^{-6}$.

are found to be oscillatory, with more-dissipative cases tending to yield more stationary steady-states. These solutions go beyond previous calculations in several ways. First, dissipative effects such as viscosity and resistivity are included, which are not present in most other numerical methods for obtaining such steady-states. These results also go beyond those obtained using other methods which do include dissipative effects, because here the numerical methods allow time-integration to be carried sufficiently far to ensure a steady-state on all physical time-scales present in the problem. Second, these simulations include realistic current drive, heating, and particle injection mechanisms, and may therefore reach a realistic steady-state in the presence of dissipation. Third, the model used here includes both parallel viscosity and gyroviscosity, which have significant influence on the steady-state flows, and which have not been included in any other study of this type. Finally, two-fluid effects are also included here, which appear not to have been present in any comparable published work.

In these solutions, a number of interesting results have been found, some of which have not previously been observed or predicted. The radial flows have been found to be in excellent agreement with the Pfirsch-Schlüter theory, as they should be. The steady-state poloidal and toroidal components of the flow, which are free functions in the non-dissipative case, are more difficult to obtain analytically, especially in general geometry, and therefore simulations such as the ones described in this work are particularly useful in this regard. The radial electric field, which determines the toroidal rotation, is naturally similarly difficult to calculate analytically, but may be easily extracted from simulation results. It is found that strong, up-down asymmetric toroidal edge flows may exist in highly resistive SOLs, in accordance with previous simulation results [3]. Parallel viscosity has been demonstrated to damp poloidal flows significantly, as previously anticipated [36]. The radial electric field has been found to be due mainly to the ion pressure gradient, with the poloidal electric and ion diamagnetic drifts therefore nearly equal and opposite, even in the absence of parallel viscosity. In the cases presented here, the surface-averaged toroidal angular momentum balance is between isotropic viscosity, gyroviscosity, and inertia (these are essentially the only torques which can contribute to the flux-averaged torque) with the dominant balance determined by the choice of parameters. The dynamical system has been found not to attain a stationary state when the torque due to isotropic viscosity is significantly smaller than either of the other two (non-dissipative) terms.

In particular, gyroviscosity is found to play an important role in the steady-state flows, driving toroidal flows in the presence of a localized particle source. A theoretical basis for this core rotation, based on the gyroviscous cancellation effect, has been presented elsewhere [33], and will be the subject of a future publication. Because the Braginskii form of gyroviscosity is valid in all collisionality regimes, this result is expected to persist under actual experimental parameters. This suggests the possibility of driving toroidal flows in fusion plasmas by pellet injection.

## Acknowledgments

We would like to acknowledge the significant and important contributions of A. Bauer, X. Luo, and the RPI SCOREC team to this project for the development of the meshing software used by M3D-C[1], and of specialized interfaces to that software. We also thank J. Ramos for informative discussions regarding the gyroviscosity. This work was supported by the US Department of Energy under Contract DE-AC02-09CH11466 and by the SciDAC Center for Extended Magnetohydrodynamic Modeling (CEMM).

## Appendix A. Normalizations

The system of units used for all quantities in this paper (unless otherwise noted) is derived from a characteristic length, density, and magnetic field. The units for various dimensional quantities are listed in the following table, along with the conversion to SI units when the characteristic quantities are given values appropriate to NSTX.

| Physical quantity | | Normalization | NSTX values |
|---|---|---|---|
| Length | $\mathbf{x}$ | $L_0$ | 1 m |
| Density | $n$ | $n_0$ | $2 \times 10^{19}$ m$^{-3}$ |
| Magnetic field | $\mathbf{B}$ | $B_0$ | 0.3 T |
| Velocity | $\mathbf{u}$ | $v_{A0} = B_0/\sqrt{4\pi m_i n_0}$ | $1.5 \times 10^6$ m/s |
| Time | $t$ | $\tau_{A0} = L_0/v_{A0}$ | 0.68 μs |
| Pressure | $p, \Pi$ | $B_0^2/4\pi$ | 0.7 atm |
| Temperature | $T$ | $B_0^2/4\pi n_0$ | 22 keV |
| Energy | $E$ | $B_0^2 L_0^3/4\pi$ | 72 kJ |
| Electric field | $\mathbf{E}$ | $v_{A0}B_0/c$ | 450 kV/m |
| Current density | $\mathbf{J}$ | $B_0\, c/4\pi L_0$ | 240 kA/m$^2$ |
| Current | $I$ | $B_0\, cL_0/4\pi$ | 240 kA |
| Resistivity | $\eta$ | $4\pi\tau_{A0}(v_{A0}/c)^2$ | 1.9 Ωm |
| Diffusivity | $D_n$ | $L_0^2/\tau_{A0}$ | $1.5 \times 10^6$ m$^2$/s |
| Viscosity | $\mu$ | $B_0^2\tau_{A0}/4\pi$ | |

**Appendix A** (*continued*)

| Physical quantity | | Normalization | NSTX values |
|---|---|---|---|
| Thermal conductivity | $\kappa$ | $n_0 L_0^2/\tau_{A0}$ | |

The expressions for the collisional (Braginskii) forms of various transport coefficients are given (in normalized units) in the following table. These expressions are for reference only, and yield neither the values used in simulations here, nor the values observed experimentally.

| Transport coefficient | Normalized expression |
|---|---|
| $\eta$ | $d_i^2(m_e/m_i)/\tau_e$ |
| $\mu_\perp^{(i)}$ | $\frac{3}{10}d_i^2 p_i/\tau_i$ |
| $\mu_\parallel^{(i)}$ | $0.96 p_i \tau_i$ |
| $\kappa_\perp^{(i)}$ | $2d_i^2 p_i/\tau_i$ |
| $\kappa_\wedge^{(i)}$ | $-\frac{5}{2}d_i p_i$ |
| $\kappa_\parallel^{(e)}$ | $3.2 p_e \tau_e/(m_e/m_i)$ |

where

$$\tau_e = \tau_i \sqrt{\frac{m_e}{2m_i}}\left(\frac{T_e}{T_i}\right)^{3/2}. \tag{40}$$

## Appendix B. Analysis of temporal discretizations

### B.1. Stability

Consider the hyperbolic system of equations

$$\frac{\partial u}{\partial t} = c\frac{\partial f}{\partial x} \tag{41}$$

$$\frac{\partial f}{\partial t} = c\frac{\partial u}{\partial x}. \tag{42}$$

Discretization of this system according to the method outlined in Section 3.2 yields

$$(1-\theta^2\delta t^2\mathcal{L})u^{n+1} = (1-\alpha\delta t^2\mathcal{L})u^n + c\,\delta t\frac{\partial f^m}{\partial x} \tag{43}$$

$$f^{m+1} = f^m + c\,\phi\,\delta t\frac{\partial u^{n+1}}{\partial x} + c\,(1-\phi)\delta t\frac{\partial u^n}{\partial x} \tag{44}$$

where $\mathcal{L} = c^2\partial_x^2$. Letting $f^{m+1} = rf^m$ and $u^{n+1} = ru^n$, the amplification factor $r$ must satisfy

$$(1+\theta^2 D)(r-1)^2 + D(\theta^2+\phi-\alpha)(r-1) + D = 0 \tag{45}$$

where $D = \delta t^2 c^2 k^2$, assuming $\partial_x = ik$. Eq. (45) has solutions

$$r = \frac{1+\frac{1}{2}D(\theta^2-\phi+\alpha) \pm i\sqrt{D+[\theta^2-\frac{1}{4}(\theta^2+\phi-\alpha)^2]D^2}}{1+\theta^2 D} \tag{46}$$

for which

$$|r|^2 = \frac{1+(1+\alpha-\theta)D}{1+\theta^2 D} \tag{47}$$

when the quantity within the square-root of Eq. (46) is nonnegative. For the Caramana method, for which $\phi = 1$ and $\alpha = \theta^2$, this means that $|r|^2 = 1$ for any $D$, as long as $\theta \geqslant \frac{1}{2}$. Thus this method is linearly stable and non-dissipative in this case when $\theta \geqslant 1/2$.

For the split $\theta$-implicit method, for which $\phi = \theta$ and $\alpha = \theta(\theta-1)$, the amplification factor is $|r|^2 = 1 + [(1-2\theta)D/(1+\theta^2 D)]$, which is less than or equal to 1 (and hence stable) when $\theta \geqslant \frac{1}{2}$. (The quantity within the square-root of Eq. (46) is exactly $D$ for this method, which is assumed to be positive.) Note that since $|r|^2 < 1$ when $\theta > \frac{1}{2}$

the split $\theta$-implicit method introduces numerical dissipation in this case; this is not true for the Caramana method, for any value of $\theta$.

### B.2. Temporal truncation error

The temporal truncation error of these discretizations may be determined by standard methods. First we consider the Caramana discretization, for which $m = n + \frac{1}{2}$, $\phi = 1$, and $\alpha = \theta^2$. Taylor expanding Eq. (43) about timestep $n$ yields

$$\begin{aligned}(1-\theta^2\delta t^2\mathcal{L})\left(u+\delta t\,\partial_t u+\frac{1}{2}\delta t^2\partial_t^2 u+\frac{1}{6}\delta t^3\partial_t^3 u+\mathcal{O}(\delta t^4)\right)\\ =(1-\theta^2\delta t^2\mathcal{L})u+\delta t\,c\,\partial_x\left[f+\left(\frac{\delta t}{2}\right)\partial_t f+\frac{1}{2}\left(\frac{\delta t}{2}\right)^2\partial_t^2 f+\frac{1}{6}\left(\frac{\delta t}{2}\right)^3\partial_t^3 f+\mathcal{O}(\delta t^4)\right].\end{aligned} \tag{48}$$

Dividing by $\delta t$ and using Eqs. (41) and (42) to eliminate $f$ (except for the $\mathcal{O}(\delta t^0)$ occurrence) yields

$$\partial_t u = c\,\partial_x f+\left(\theta^2-\frac{1}{24}\right)\delta t^2\partial_t^3 u+\mathcal{O}(\delta t^3). \tag{49}$$

Similarly, Eq. (44) becomes

$$\partial_t f = c\,\partial_x u-\frac{1}{24}\delta t^2\partial_t^3 f+\mathcal{O}(\delta t^3). \tag{50}$$

(This can be seen immediately by noting that Eq. (44) has the same form as Eq. (43) with $\theta = 0$.) Therefore the Caramana time discretization is second-order accurate for any stable value of $\theta$.

An identical analysis of the split $\theta$-implicit method yields

$$\partial_t u = c\,\partial_x f+\left(\theta-\frac{1}{2}\right)\delta t\,\partial_t^2 u+\left(\theta^2-\frac{1}{6}\right)\delta t^2\partial_t^3 u+\mathcal{O}(\delta t^3)$$

$$\partial_t f = c\,\partial_x u+\left(\theta-\frac{1}{2}\right)\delta t\,\partial_t^2 f+\frac{1}{2}\left(\theta-\frac{1}{3}\right)\delta t^2\partial_t^3 f+\mathcal{O}(\delta t^3).$$

Thus the split $\theta$-implicit method is second-order accurate only for $\theta = \frac{1}{2}$.

### B.3. Accuracy of stationary solutions

While the short-timescale dynamics of the magnetohydrodynamic system considered in the main text are dominantly hyperbolic in character, the parabolic terms will necessarily play an important role in the stationary solutions of the system, and must be included in any assessment of the accuracy of the stationary solutions to the discretized equations. Therefore, we consider a more general set of equations which include dissipation:

$$\frac{\partial u}{\partial t} = c\frac{\partial f}{\partial x}+\mu\frac{\partial^2 u}{\partial x^2} \tag{51}$$

$$\frac{\partial f}{\partial t} = c\frac{\partial u}{\partial x}+\eta\frac{\partial^2 f}{\partial x^2}. \tag{52}$$

The general stationary solution to these continuous equations is

$$u_s(x) = u_0+[A\cosh(kx)+B\sinh(kx)] \tag{53}$$

$$f_s(x) = f_0-\frac{c}{k\eta}[B\cosh(kx)+A\sinh(kx)] \tag{54}$$

where $k = c/\sqrt{\eta\mu}$ and $A, B, u_0$, and $f_0$ are arbitrary constants of integration. The Caramana discretization of Eqs. (51) and (52) is

$$(1-\theta^2\delta t^2\mathcal{L}-\theta\,\mu\,\delta t)u^{n+1} = (1-\theta^2\delta t^2\mathcal{L}-\theta\,\mu\,\delta t)u^n+\mu\,\delta t\frac{\partial^2 u^n}{\partial x^2}+c\,\delta t\frac{\partial f^{n+\frac{1}{2}}}{\partial x} \tag{55}$$

$$(1-\theta\,\eta\,\delta t)f^{n+\frac{3}{2}} = (1-\theta\,\eta\,\delta t)f^{n+\frac{1}{2}}+\eta\,\delta t\frac{\partial^2 f^{n+\frac{1}{2}}}{\partial x^2}+c\,\delta t\frac{\partial u^{n+1}}{\partial x}. \tag{56}$$

It is found that letting $u^{n+1} = u^n = u_s(x)$ and $f^{n+\frac{3}{2}} = f^{n+\frac{1}{2}} = f_s(x)$ satisfies Eqs. (55) and (56) exactly, and therefore the Caramana discrete-time equations admit the same stationary solutions and the continuous-time equations, regardless of the choice of $\theta$.

In contrast, the split $\theta$-implicit discretization is

$$(1-\theta^2\delta t^2\mathcal{L}-\theta\mu\delta t)u^{n+1} = (1-\theta(\theta-1)\delta t^2\mathcal{L}-\theta\mu\delta t)u^n + \mu\delta t\frac{\partial^2 u^n}{\partial x^2} + c\,\delta t\frac{\partial f^{n+\frac{1}{2}}}{\partial x} \tag{57}$$

$$(1-\theta\eta\delta t)f^{n+1} = (1-\theta\eta\delta t)f^n + \eta\delta t\frac{\partial^2 f^n}{\partial x^2} + c\,\delta t\frac{\partial u^{n+1}}{\partial x}. \tag{58}$$

While Eq. (58) is satisfied exactly by $f^{n+1} = f^n = f_s(x)$ and $u^{n+1} = u^n = u_s(x)$, Eq. (57) is not. It is found that the general solution to Eqs. (57) and (58) is obtained by replacing $k$ with $\kappa = c/\sqrt{\eta\mu + \eta c^2\theta\,\delta t}$ everywhere in Eqs. (53) and (54). Note that $|\kappa| < |k|$, which is consistent with the observation that the term dropped in the Caramana method is responsible for an artificial numerical diffusion [30]. Thus there is an $\mathcal{O}(\delta t)$ error in the stationary solution to the $\theta$-implicit split discretization. This $\mathcal{O}(\delta t)$ error in the stationary solution persists even in the case where $\theta = 1/2$, in which case the dynamical error of the split $\theta$-implicit discretization is $\mathcal{O}(\delta t^2)$. The results presented in Fig. 2 are in agreement with the analysis of this section.

## Appendix C. Scalar form of equations implemented in M3D-C[1]

In this section, the scalar forms of the physical equations, Eqs. (1)–(5) are presented. The scalar forms of the time-advance equations derived in Section 3.2.

Before proceeding, the following definitions are made to simplify notation:

$$\Delta^* a = R^2\nabla\cdot\left(\frac{\nabla a}{R^2}\right)$$
$$\langle a,b\rangle = \nabla a\cdot\nabla b$$
$$[a,b] = \nabla\varphi\cdot\nabla a\times\nabla b$$
$$\langle\langle a,b\rangle\rangle = \nabla\nabla a : \nabla\nabla b$$
$$[\langle a,b\rangle] = \nabla\varphi\cdot\nabla\nabla a\dot{\times}\nabla\nabla b$$
$$[[a,b]] = \nabla\varphi\cdot\nabla\nabla a\overset{\times}{\times}\nabla\nabla b\cdot\nabla\varphi.$$

For compactness, derivatives are written as subscripts in the following expressions (i.e. $v_Z = \partial_Z v$).

Writing the magnetic field and velocity in the flux/potential form of Eqs. (31) and (32), (1) and (4) may be written:

$$\dot n = -[n,U] - \langle n,\chi\rangle - n\nabla^2\chi + \sigma + \nabla\cdot(D_n\nabla n), \tag{59}$$

$$\dot p = -[p,U] - \langle p,\chi\rangle - \Gamma p\nabla^2\chi - \frac{d_i}{n}[I,p_e] - d_i\Gamma p_e\left[I,\frac{1}{n}\right] + (\Gamma-1)\left[d_i\mathbf{R}\cdot\frac{\mathbf{J}}{n} + d_i\Pi_e : \nabla\frac{\mathbf{J}}{n} - \nabla\cdot\mathbf{q}\right]. \tag{60}$$

Acting on Eq. (2) with the operators $-\nabla\varphi\cdot\nabla\times, R^2\nabla\varphi\cdot$, and $\nabla\cdot$ yields:

$$\begin{aligned} n\Delta^*\dot U + \langle n,\dot U\rangle - R^2[n,\dot\chi] = {} & R^2\left[\frac{\Delta^*\psi}{R^2},\psi\right] + \left(\frac{I^2}{R^2}\right)_Z - R^2\left[n\frac{\Delta^* U}{R^2},U\right] - \frac{R^2}{2}\left[\frac{\langle U,U\rangle}{R^2},n\right] - \frac{\left(nV^2\right)_Z}{R^2} - \langle n\Delta^* U,\chi\rangle - n\Delta^* U\Delta^*\chi \\ & - R^2[n,[U,\chi]] - \frac{1}{2}R^2[\langle\chi,\chi\rangle,n] - \sigma\Delta^* U - \langle\sigma,U\rangle + R^2[\sigma,\chi] - R^2\nabla\varphi\cdot\nabla\times(n\mathbf{g} - \nabla\cdot\Pi) \end{aligned} \tag{61}$$

$$n\dot V = [I,\psi] - n[V,U] - n\langle V,\chi\rangle - \sigma V + R^2\nabla\varphi\cdot(n\mathbf{g} - \nabla\cdot\Pi) \tag{62}$$

$$\begin{aligned} n\nabla^2\dot\chi + \langle n,\dot\chi\rangle + [n,\dot U] = {} & -\nabla^2 p - \frac{1}{R^2}[(\Delta^*\psi)^2 + \langle\Delta^*\psi,\psi\rangle] - \frac{1}{2R^2}\Delta^*(I^2) + \frac{1}{R^2}[n(\Delta^* U)^2 + \langle n\Delta^* U,U\rangle] \\ & - \frac{1}{2}\left[n\nabla^2\left(\frac{\langle U,U\rangle}{R^2}\right) + \langle n,\frac{\langle U,U\rangle}{R^2}\rangle\right] + \frac{1}{R}\left(\frac{nV^2}{R^2}\right)_R - n\nabla^2[\chi,U] - [n\Delta^* U,\chi] + \langle n,[U,\chi]\rangle \\ & - \frac{1}{2}(n\nabla^2\langle\chi,\chi\rangle + \langle n,\langle\chi,\chi\rangle\rangle) - [\sigma,U] - \sigma\nabla^2\chi - \langle\sigma,\chi\rangle + \nabla\cdot(n\mathbf{g} - \nabla\cdot\Pi) \end{aligned} \tag{63}$$

The scalar equation for the time-evolution of the magnetic flux and toroidal field may be found by operating on Eqs. (7) and (5) with $R^2\nabla\varphi\cdot$, respectively:

$$\dot\psi = -[\psi,U] - \langle\psi,\chi\rangle + \frac{d_i}{n}[\psi,I] - \frac{d_i}{n}R^2\nabla\varphi\cdot(\mathbf{R} - \nabla\cdot\Pi_e) \tag{64}$$

$$\dot{I} = -R^2\left[\frac{I}{R^2}, U\right] - R^2\left[\psi, \frac{V}{R^2}\right] - I\Delta^*\chi - \langle I, \chi\rangle + R^2 d_i\left(\left[\frac{\Delta^*\psi}{R^2 n}, \psi\right] + \frac{1}{2}\left[\frac{1}{R^2 n}, I^2\right] + \left[\frac{1}{n}, p_e\right]\right) - R^2\nabla\varphi\cdot\nabla\times\left[\frac{d_i}{n}(\mathbf{R} - \nabla\cdot\Pi_e)\right], \tag{65}$$

The scalar form of $\nabla\cdot\Pi$ is not expanded here, as it contains derivative of greater than second order and is therefore not useful in this form. The scalar form of this term after integration by parts is written in the following section.

### C.1. Weak form

Eqs. (59)–(65) may now be Taylor expanded and discretized in the exactly the same manner as Eqs. (1)–(5) were in Section 3.2. These scalar equations may then be integrated to yield the weak equations appropriate for computation with finite elements. The final result of this process is the set of matrix Eqs. (33)–(36). The operators comprising the elements of the matrices in those equations are defined below.

#### C.1.1. Vorticity equation

$$\begin{aligned} S_{UU}U^x = {} & U_{Un}(U^x, n) - \theta\,\delta t\left[U_{UUn}(U^x, U, n) + U_{UUn}(U, U^x, n) + U_{U\chi n}(U^x, \chi, n) + U_{U\Pi}(U^x) + U_{U\sigma}(U^x)\right] \\ & - \theta^2\delta t^2\left[U_{U\psi\psi}(U^x, \psi, \psi) + U_{UII}(U^x, I, I) + U_{Un\mathbf{g}}(U^x, n)\right] \end{aligned} \tag{66}$$

$$S_{UV}V^x = -\theta\,\delta t[lU_{VVn}(V^x, V, n) + U_{VVn}(V, V^x, n) + U_{V\Pi}(V^x)] - \theta^2\delta t^2[U_{V\psi I}(V^x, \psi, I)] \tag{67}$$

$$\begin{aligned} S_{U\chi}\chi^x = {} & U_{\chi n}(\chi^x, n) - \theta\,\delta t\left[U_{\chi\chi n}(\chi^x, \chi, n) + U_{\chi\chi n}(\chi, \chi^x, n) + U_{U\chi n}(U, \chi^x, n) + U_{\chi\Pi}(\chi^x) + V_{\chi\sigma}(\chi^x)\right] \\ & - \theta^2\delta t^2\left[U_{\chi\psi\psi}(\chi^x, \psi, \psi) + U_{\chi II}(\chi^x, I, I) + U_{\chi n\mathbf{g}}(\chi^x, n)\right] \end{aligned} \tag{68}$$

$$\begin{aligned} D_{UU}U^x = {} & U_{Un}(U^x, n) + (1-\theta)\delta t[U_{U\Pi}(U^x) + U_{U\sigma}(U^x)] + \left(\frac{1}{2} - \theta\right)\delta t\left[U_{UUn}(U^x, U, n) + U_{UUn}(U, U^x, n) + U_{U\chi n}(U^x, \chi, n)\right] \\ & + \frac{1}{2}\delta t\left[U_{UUn}(U^x, U^0, n) + U_{UUn}(U^0, U^x, n) + U_{U\chi n}(U^x, \chi^0, n)\right] - \theta^2\delta t^2\left[U_{U\psi\psi}(U^x, \psi, \psi) + U_{UII}(U^x, I, I) + U_{U\mathbf{g}}(U^x)\right] \end{aligned} \tag{69}$$

$$\begin{aligned} D_{UV}V^x = {} & (1-\theta)\delta t[U_{V\Pi}(V^x)] + \left(\frac{1}{2} - \theta\right)\delta t[U_{VVn}(V^x, V, n) + U_{VVn}(V, V^x, n)] + \frac{1}{2}\delta t[U_{VVn}(V^x, V^0, n) + U_{VVn}(V^0, V^x, n)] \\ & - \theta^2\delta t^2[U_{V\psi I}(V^x, \psi, I)] \end{aligned} \tag{70}$$

$$\begin{aligned} D_{U\chi}\chi^x = {} & U_{\chi n}(\chi^x, n) + (1-\theta)\delta t[U_{\chi\Pi}(\chi^x) + U_{\chi\sigma}(\chi^x)] + \left(\frac{1}{2} - \theta\right)\delta t\left[U_{\chi\chi n}(\chi^x, \chi, n) + U_{\chi\chi n}(\chi, \chi^x, n) + U_{U\chi n}(U, \chi^x, n)\right] \\ & + \frac{1}{2}\delta t\left[U_{\chi\chi n}(\chi^x, \chi^0, n) + U_{\chi\chi n}(\chi^0, \chi^x, n) + U_{U\chi n}(U^0, \chi^x, n)\right] - \theta^2\delta t^2\left[U_{\chi\psi\psi}(\chi^x, \psi, \psi) + U_{\chi II}(\chi^x, I, I) + U_{\chi n\mathbf{g}}(\chi^x, n)\right] \end{aligned} \tag{71}$$

$$\begin{aligned} Q_{U\psi}\psi^x = {} & \frac{1}{2}\delta t\left[U_{\psi\psi}(\psi^x, \psi + \psi^0) + U_{\psi\psi}(\psi + \psi^0, \psi^x)\right] \\ & - \frac{1}{2}\theta^2\delta t^2\left[U_{U\psi\psi}(U^0, \psi^x, \psi + \psi^0) + U_{U\psi\psi}(U^0, \psi + \psi^0, \psi^x)U_{\chi\psi\psi}(\chi^0, \psi^x, \psi + \psi^0) + U_{\chi\psi\psi}(\chi^0, \psi + \psi^0, \psi^x) + U_{V\psi I}(V^0, \psi^x, I + I^0)\right] \end{aligned} \tag{72}$$

$$\begin{aligned} Q_{UI}I^x = {} & \frac{1}{2}\delta t\left[U_{II}(I^x, I + I^0) + U_{II}(I + I^0, I^x)\right] \\ & - \frac{1}{2}\theta^2\delta t^2\left[U_{UII}(U^0, I^x, I + I^0) + U_{UII}(U^0, I + I^0, I^x)U_{\chi II}(\chi^0, I^x, I + I^0) + U_{\chi II}(\chi^0, I + I^0, I^x) + U_{V\psi I}(V^0, \psi + \psi^0, I^x)\right] \end{aligned} \tag{73}$$

$$Q_{Up}p^x = 0 \tag{74}$$

$$\begin{aligned} Q_{Un}n^x = {} & \delta t\left[U_{UUn}(U^0, U^0, n^x) + U_{VVn}(V^0, V^0, n^x) + U_{\chi\chi n}(\chi^0, \chi^0, n^x) + U_{U\chi n}(U^0, \chi^0, n^x) + U_{n\mathbf{g}}(n^x)\right] \\ & + \delta t^2\left[U_{Un\mathbf{g}}(U^0, n^x) + U_{\chi n\mathbf{g}}(\chi^0, n^x)\right] \end{aligned} \tag{75}$$

*C.1.2. Toroidal velocity equation*

$$S_{VU}U^x = -\theta\,\delta t[V_{UVn}(U^x,V,n)+V_{U\Pi}(U^x)] - \theta^2\delta t^2[V_{U\psi I}(U^x,\psi,I)] \tag{76}$$

$$S_{VV}V^x = V_{Vn}(V^x,n) - \theta\,\delta t\left[V_{UVn}(U,V^x,n)+V_{V\chi n}(V^x,\chi,n)+V_{V\Pi}(V^x)+V_{V\sigma}(V^x)\right] - \theta^2\delta t^2[V_{V\psi\psi}(V^x,\psi,\psi)] \tag{77}$$

$$S_{V\chi}\chi^x = -\theta\,\delta t[V_{V\chi n}(V,\chi^x,n)+V_{\chi\Pi}(\chi^x)] - \theta^2\delta t^2[V_{\chi\psi I}(\chi^x,\psi,I)] \tag{78}$$

$$D_{VU}U^x = (1-\theta)\delta t[V_{U\Pi}(U^x)] + \left(\frac{1}{2}-\theta\right)\delta t[V_{UVn}(U^x,V,n)] + \frac{1}{2}\delta t[V_{UVn}(U^x,V^0,n)] - \theta^2\delta t^2[V_{U\psi I}(U^x,\psi,I)] \tag{79}$$

$$\begin{aligned} D_{VV}V^x = {} & V_{Vn}(V^x,n)(1-\theta)\delta t[V_{V\Pi}(V^x)+V_{V\sigma}(V^x)]\left(\frac{1}{2}-\theta\right)\delta t[V_{UVn}(U,V^x,n)+V_{V\chi n}(V^x,\chi,n)] + \frac{1}{2}\delta t[V_{UVn}(U^0,V^x,n) \\ & + V_{V\chi n}(V^x,\chi^0,n)] - \theta^2\delta t^2[V_{V\psi\psi}(V^x,\psi,\psi)] \end{aligned} \tag{80}$$

$$D_{V\chi}\chi^x = (1-\theta)\delta t[V_{\chi\Pi}(\chi^x)] + \left(\frac{1}{2}-\theta\right)\delta t[V_{V\chi n}(V,\chi^x,n)] + \frac{1}{2}\delta t[V_{V\chi n}(V^0,\chi^x,n)] - \theta^2\delta t^2[V_{\chi\psi I}(\chi^x,\psi,I)] \tag{81}$$

$$\begin{aligned} Q_{V\psi}\psi^x = {} & \frac{1}{2}\delta t\left[V_{\psi I}(\psi^x,I+I^0)\right] \\ & + \frac{1}{2}\theta\,\delta t^2\left[IV_{V\psi\psi}(V^0,\psi+\psi^0,\psi^x)+V_{V\psi\psi}(V^0,\psi^x,\psi+\psi^0)+U_{U\psi I}(U^0,\psi^x,I+I^0)+U_{\chi\psi I}(\chi^0,\psi^x,I+I^0)\right] \end{aligned} \tag{82}$$

$$Q_{VI}I^x = \frac{1}{2}\delta t[V_{\psi I}(\psi+\psi^0,I^x)] + \frac{1}{2}\theta\,\delta t^2\left[U_{U\psi I}(U^0,\psi+\psi^0,I^x)+U_{\chi\psi I}(\chi^0,\psi+\psi^0,I^x)\right] \tag{83}$$

$$Q_{Vp}p^x = 0 \tag{84}$$

$$Q_{Vn}n^x = \delta t[V_{UVn}(U^0,V^0,n^x)+V_{V\chi n}(V^0,\chi^0,n^x)] \tag{85}$$

*C.1.3. Compressional velocity equation*

$$\begin{aligned} S_{\chi U}U^x = {} & X_{Un}(U^x,n) - \theta\,\delta t\left[X_{UUn}(U^x,U,n)+X_{UUn}(U,U^x,n)+X_{U\chi n}(U^x,\chi,n)+X_{U\Pi}(U^x)+X_{U\sigma}(U^x)\right] \\ & - \theta^2\delta t^2\left[X_{U\psi\psi}(U^x,\psi,\psi)+X_{UII}(U^x,I,I)+X_{Up}(U^x,p)+X_{Un\mathbf{g}}(U^x,n)\right] \end{aligned} \tag{86}$$

$$S_{\chi V}V^x = -\theta\,\delta t[X_{VVn}(V^x,V,n)+X_{VVn}(V,V^x,n)+X_{V\Pi}(V^x)] - \theta^2\delta t^2\left[X_{V\psi I}(V^x,\psi,I)\right] \tag{87}$$

$$\begin{aligned} S_{U\chi}\chi^x = {} & X_{\chi n}(\chi^x,n) - \theta\,\delta t\left[X_{\chi\chi n}(\chi^x,\chi,n)+X_{\chi\chi n}(\chi,\chi^x,n)+X_{U\chi n}(U,\chi^x,n)+X_{\chi\Pi}(\chi^x)+X_{\chi\sigma}(\chi^x)\right] \\ & - \theta^2\delta t^2\left[X_{\chi\psi\psi}(\chi^x,\psi,\psi)+X_{\chi II}(\chi^x,I,I)+X_{\chi p}(\chi^x,p)+X_{\chi\mathbf{g}}(\chi^x)\right] \end{aligned} \tag{88}$$

$$\begin{aligned} D_{\chi U}U^x = {} & X_{Un}(U^x,n)+(1-\theta)\delta t[X_{U\Pi}(U^x)+X_{U\sigma}(U^x)]+\left(\frac{1}{2}-\theta\right)\delta t\left[X_{UUn}(U^x,U,n)+X_{UUn}(U,U^x,n)+X_{U\chi n}(U^x,\chi,n)\right] \\ & + \frac{1}{2}\delta t\left[X_{UUn}(U^x,U^0,n)+X_{UUn}(U^0,U^x,n)+X_{U\chi n}(U^x,\chi^0,n)\right] - \theta^2\delta t^2\left[X_{U\psi\psi}(U^x,\psi,\psi)+X_{UII}(U^x,I,I)+X_{Up}(U^xp)+X_{Un\mathbf{g}}(U^x,n)\right] \end{aligned} \tag{89}$$

$$\begin{aligned} D_{\chi V}V^x = {} & (1-\theta)\delta t[X_{V\Pi}(V^x)]\left(\frac{1}{2}-\theta\right)\delta t[X_{VVn}(V^x,V,n)+X_{VVn}(V,V^x,n)] + \frac{1}{2}\delta t[X_{VVn}(V^x,V^0,n)+X_{VVn}(V^0,V^x,n)] \\ & - \theta^2\delta t^2[X_{V\psi I}(V^x,\psi,I)] \end{aligned} \tag{90}$$

$$\begin{aligned} D_{\chi\chi}\chi^x = {} & X_{\chi n}(\chi^x,n)+(1-\theta)\delta t[X_{\chi\Pi}(\chi^x)+X_{\chi\sigma}(\chi^x)]+\left(\frac{1}{2}-\theta\right)\delta t\left[X_{\chi\chi n}(\chi^x,\chi,n)+X_{\chi\chi n}(\chi,\chi^x,n)+X_{U\chi n}(U,\chi^x,n)\right] \\ & + \frac{1}{2}\delta t\left[X_{\chi\chi n}(\chi^x,\chi^0,n)+X_{\chi\chi n}(\chi^0,\chi^x,n)+X_{U\chi n}(U^0,\chi^x,n)\right] \\ & - \theta^2\delta t^2\left[X_{\chi\psi\psi}(\chi^x,\psi,\psi)+X_{\chi II}(\chi^x,I,I)+X_{\chi p}(\chi,p)+X_{\chi n\mathbf{g}}(\chi^x n)\right] \end{aligned} \tag{91}$$

$$Q_{\chi\psi}\psi^x = \frac{1}{2}\delta t\left[X_{\psi\psi}(\psi^x,\psi+\psi^0)+X_{\psi\psi}(\psi+\psi^0,\psi^x)\right] - \frac{1}{2}\theta^2\delta t^2\left[X_{U\psi\psi}(U^0,\psi^x,\psi+\psi^0)+X_{U\psi\psi}(U^0,\psi+\psi^0,\psi^x)+X_{\chi\psi\psi}(\chi^0,\psi^x,\psi+\psi^0)+X_{\chi\psi\psi}(\chi^0,\psi+\psi^0,\psi^x)+X_{V\psi I}(V^0,\psi^x,I+I^0)\right] \tag{92}$$

$$Q_{\chi I}I^x = \frac{1}{2}\delta t\left[X_{II}(I^x,I+I^0)+X_{II}(I+I^0,I^x)\right] - \frac{1}{2}\theta^2\delta t^2\left[X_{UII}(U^0,I^x,I+I^0)+X_{UII}(U^0,I+I^0,I^x)X_{\chi II}(\chi^0,I^x,I+I^0)+X_{\chi II}(\chi^0,I+I^0,I^x)+X_{V\psi I}(V^0,\psi+\psi^0,I^x)\right] \tag{93}$$

$$Q_{\chi p}p^x = \delta t[X_p(p^x)] + \theta\,\delta t^2\left[X_{Up}(U^0,p^x)+X_{\chi p}(\chi^0,p^x)\right] \tag{94}$$

$$Q_{\chi n}n^x = \delta t\left[X_{UUn}(U^0,U^0,n^x)+X_{VVn}(V^0,V^0,n^x)+X_{\chi\chi n}(\chi^0,\chi^0,n^x)+X_{U\chi n}(U^0,\chi^0,n^x)+X_{n\mathbf{g}}(n^x)\right]+\delta t^2[X_{Un\mathbf{g}}(U^0,n^x) + X_{\chi n\mathbf{g}}(\chi^0,n^x)] \tag{95}$$

### C.1.4. Density equation

$$S_{nn}n^x = N_n(n^x) - \theta\,\delta t[N_{nU}(n^x,U)+N_{n\chi}(n^x,\chi)+N_{nD_n}(n^x)] \tag{96}$$

$$D_{nn}n^x = N_n(n^x) + (1-\theta)\delta t[N_{nU}(n^x,U)+N_{n\chi}(n^x,\chi)+N_{nD_n}(n^x)] \tag{97}$$

$$R_{nU}U^x = \phi\,\delta t[N_{nU}(n,U^x)] \tag{98}$$

$$R_{nV}V^x = 0 \tag{99}$$

$$R_{n\chi}\chi^x = \phi\,\delta t[N_{n\chi}(n,\chi^x)] \tag{100}$$

$$Q_{nU}U^x = (1-\phi)\delta t[N_{nU}(n,U^x)] + \delta t[N_{nU}(n^0,U^x)] \tag{101}$$

$$Q_{nV}V^x = 0 \tag{102}$$

$$Q_{n\chi}\chi^x = (1-\phi)\delta t\left[N_{n\chi}(n,\chi^x)\right] + \delta t[N_{n\chi}(n^0,\chi^x)] \tag{103}$$

### C.1.5. Pressure equation

$$S_{pp}p^x = P_p(p^x) - \theta\,\delta t\left[P_{pU}(p^x,U)+P_{p\chi}(p^x,\chi)+P_{p\kappa}(p^x)+P_{pI\kappa}(p^x,I)+P_{p\psi\psi\kappa}(p^x,\psi,\psi)\right] \tag{104}$$

$$D_{pp}p^x = P_p(p^x) + (1-\theta)\delta t\left[P_{pU}(p^x,U)+P_{p\chi}(p^x,\chi)+P_{p\kappa}(p^x)+P_{pI\kappa}(p^x,I)+P_{p\psi\psi\kappa}(p^x,\psi,\psi)\right] \tag{105}$$

$$R_{pU}U^x = \phi\,\delta t\left[P_{pU}(p,U^x)+P_{U\chi\sigma}(U^x,\chi)+P_{UU\sigma}(U^x,U)+P_{UU\sigma}(U,U^x)\right] \tag{106}$$

$$R_{pV}V^x = \phi\,\delta t[P_{VV\sigma}(V^x,V)+P_{VV\sigma}(V,V^x)] \tag{107}$$

$$R_{p\chi}\chi^x = \phi\,\delta t\left[lP_{p\chi}(p,\chi^x)+P_{U\chi\sigma}(U^x,\chi,\sigma)+P_{\chi\chi\sigma}(\chi^x,\chi)+P_{\chi\chi\sigma}(\chi,\chi^x)\right] \tag{108}$$

$$Q_{pU}U^x = (1-\phi)\delta t[P_{pU}(p,U^x)] + \delta t[P_{pU}(p^0,U^x)] + \left(\frac{1}{2}-\phi\right)\delta t\left[P_{U\chi\sigma}(U^x,\chi)+P_{UU\sigma}(U^x,U)+P_{UU\sigma}(U,U^x)\right]\frac{1}{2}\delta t\left[P_{U\chi\sigma}(U^x,\chi^0)+P_{UU\sigma}(U^x,U^0)+P_{UU\sigma}(U^0,U^x)\right] \tag{109}$$

$$Q_{pV}V^x = \left(\frac{1}{2}-\phi\right)\delta t[P_{VV\sigma}(V^x,V)+P_{VV\sigma}(V,V^x)] + \frac{1}{2}\delta t[P_{VV\sigma}(V^x,V^0)+P_{VV\sigma}(V^0,V^x)] \tag{110}$$

$$Q_{p\chi}\chi^x = (1-\phi)\delta t[P_{p\chi}(p,\chi^x)] + \delta t[P_{p\chi}(p^0,\chi^x)] + \left(\frac{1}{2}-\phi\right)\delta t\left[P_{U\chi\sigma}(U,\chi^x)+P_{\chi\chi\sigma}(\chi^x,\chi)+P_{\chi\chi\sigma}(\chi,\chi^x)\right]\frac{1}{2}\delta t\left[P_{U\chi\sigma}(U^0,\chi^x)+P_{\chi\chi\sigma}(\chi^x,\chi^0)+P_{\chi\chi\sigma}(\chi^0,\chi^x)\right] \tag{111}$$

$$O_p = \delta t\left[P_{p_e I}(p_e, I) + P_{\psi\psi\eta}(\psi,\psi) + P_{II\eta}(I,I)\right] \tag{112}$$

### C.1.6. Electron pressure equation

$$S_{p_e\psi}\psi^x = -\theta\,\delta t\left[P_{\psi\psi\eta}(\psi^x,\psi) + P_{\psi\psi\eta}(\psi,\psi^x) + P_{p\psi\psi\kappa}(p_e,\psi^x,\psi) + P_{p\psi\psi\kappa}(p_e,\psi,\psi^x)\right] \tag{113}$$

$$S_{p_e I}I^x = -\theta\,\delta t\left[P_{II\eta}(I^x,I) + P_{II\eta}(I,I^x) + P_{p_e I}(p_e,I^x) + P_{pI\kappa}(p_e,I^x)\right] \tag{114}$$

$$S_{p_e p_e}p_e^x = P_p(p_e^x) - \theta\,\delta t\left[P_{pU}(p_e^x,U) + P_{p\chi}(p_e^x,\chi) + P_{p_e I}(p_e^x,I) + P_{p\kappa}(p_e^x) + P_{pI\kappa}(p_e^x,I) + P_{p\psi\psi\kappa}(p_e^x,\psi,\psi)\right] \tag{115}$$

$$\begin{aligned} D_{p_e\psi}\psi^x = {} & \left(\frac{1}{2}-\theta\right)\delta t\left[P_{\psi\psi\eta}(\psi^x,\psi) + P_{\psi\psi\eta}(\psi,\psi^x) + P_{p\psi\psi\kappa}(p_e,\psi^x,\psi) + P_{p\psi\psi\kappa}(p_e,\psi,\psi^x)\right] \\ & + \frac{1}{2}\delta t\left[P_{\psi\psi\eta}(\psi^x,\psi^0) + P_{\psi\psi\eta}(\psi^0,\psi^x) + P_{p\psi\psi\kappa}(p_e,\psi^x,\psi^0) + P_{p\psi\psi\kappa}(p_e,\psi^0,\psi^x)\right] \end{aligned} \tag{116}$$

$$\begin{aligned} D_{p_e I}I^x = {} & -\theta\,\delta t[P_{p_e I}(p_e,I^x) + P_{pI\kappa}(p_e,I^x)] + \delta t[P_{p_e I}(p_e^0,I^x) + P_{pI\kappa}(p_e^0,I^x)] + \left(\frac{1}{2}-\theta\right)\delta t[P_{II\eta}(I^x,I) + P_{II\eta}(I,I^x)] \\ & + \frac{1}{2}\delta t[P_{II\eta}(I^x,I^0) + P_{II\eta}(I^0,I^x)] \end{aligned} \tag{117}$$

$$D_{p_e p_e}p_e^x = P_p(p_e^x) + (1-\theta)\delta t\left[P_{pU}(p_e^x,U) + P_{p\chi}(p_e^x,\chi) + P_{p_e I}(p_e^x,I) + P_{p\kappa}(p_e^x) + P_{pI\kappa}(p_e^x,I) + P_{p\psi\psi\kappa}(p_e^x,\psi,\psi)\right] \tag{118}$$

$$R_{p_e U}U^x = \phi\,\delta t[P_{pU}(p_e,U^x)] \tag{119}$$

$$R_{p_e V}V^x = 0 \tag{120}$$

$$R_{p_e\chi}\chi^x = \phi\,\delta t[P_{p\chi}(p_e,\chi^x)] \tag{121}$$

$$Q_{p_e U}U^x = (1-\phi)\delta t[P_{pU}(p_e,U^x)] + \delta t[P_{pU}(p_e^0,U^x)] \tag{122}$$

$$Q_{p_e V}V^x = 0 \tag{123}$$

$$Q_{p_e\chi}\chi^x = (1-\phi)\delta t[P_{p\chi}(p_e,\chi^x)] + \delta t[P_{p\chi}(p_e^0,\chi^x)] \tag{124}$$

$$O_{p_e} = 0 \tag{125}$$

### C.1.7. Magnetic flux equation

$$S_{\psi\psi}\psi^x = \Psi_\psi(\psi^x) - \theta\,\delta t\left[\Psi_{\psi U}(\psi^x,U) + \Psi_{\psi\chi}(\psi^x,\chi) + \Psi_{\psi I}(\psi^x,I) + \Psi_{\psi\eta}(\psi^x)+\right] \tag{126}$$

$$S_{\psi I}I^x = -\theta\,\delta t[\Psi_{\psi I}(\psi,I^x)] \tag{127}$$

$$S_{\psi p_e}p_e^x = 0 \tag{128}$$

$$D_{\psi\psi}\psi^x = \Psi_\psi(\psi^x)(1-\theta)\delta t\left[\Psi_{\psi U}(\psi^x,U) + \Psi_{\psi\chi}(\psi^x,\chi) + \Psi_{\psi\eta}(\psi^x)+\right] + \left(\frac{1}{2}-\theta\right)\delta t[\Psi_{\psi I}(\psi^x,I)] + \frac{1}{2}\delta t[\Psi_{\psi I}(\psi^x,I^0)] \tag{129}$$

$$D_{\psi I}I^x = \left(\frac{1}{2}-\theta\right)\delta t[\Psi_{\psi I}(\psi,I^x)] + \frac{1}{2}\delta t[\Psi_{\psi I}(\psi^0,I^x)] \tag{130}$$

$$D_{\psi p_e}p_e^x = 0 \tag{131}$$

$$R_{\psi U}U^x = \phi\,\delta t[\Psi_{\psi U}(\psi,U^x)] \tag{132}$$

$$R_{\psi V}V^x = 0 \tag{133}$$

$$R_{\psi\chi}\chi^x = \phi\,\delta t[\Psi_{\psi\chi}(\psi,\chi^x)] \tag{134}$$

$$Q_{\psi U}U^x = -\phi\,\delta t[\Psi_{\psi U}(\psi, U^x)] + \delta t[\Psi_{\psi U}(\psi^0, U^x)] \tag{135}$$

$$Q_{\psi V}V^x = 0 \tag{136}$$

$$Q_{\psi\chi}\chi^x = -\phi\,\delta t[\Psi_{\psi\chi}(\psi, \chi^x)] + \delta t[\Psi_{\psi\chi}(\psi^0, \chi^x)] \tag{137}$$

*C.1.8. Toroidal magnetic field equation*

$$S_{I\psi}\psi^x = -\theta\,\delta t\left[I_{\psi\psi}(\psi^x, \psi) + I_{\psi\psi}(\psi, \psi^x) + I_{\psi V}(\psi^x, V)\right] \tag{138}$$

$$S_{II}I^x = I_I(I^x) - \theta\,\delta t\left[I_{IU}(I^x, U) + I_{I\chi}(I^x, \chi) + I_{I\eta}(I^x) + I_{II}(I^x, I) + I_{II}(I, I^x)\right] \tag{139}$$

$$S_{Ip_e}p_e^x = -\theta\,\delta t[I_{p_e}(p_e^x)] \tag{140}$$

$$D_{I\psi}\psi^x = (1-\theta)\delta t[I_{\psi V}(\psi^x, V)] + \left(\frac{1}{2} - \theta\right)\delta t[I_{\psi\psi}(\psi^x, \psi) + I_{\psi\psi}(\psi, \psi^x)] + \frac{1}{2}\delta t[I_{\psi\psi}(\psi^x, \psi^0) + I_{\psi\psi}(\psi^0, \psi^x)] \tag{141}$$

$$D_{II}I^x = I_I(I^x) + (1-\theta)\delta t\left[I_{IU}(I^x, U) + I_{I\chi}(I^x, \chi) + I_{I\eta}(I^x)\right] + \left(\frac{1}{2} - \theta\right)\delta t[I_{II}(I^x, I) + I_{II}(I, I^x)] + \frac{1}{2}\delta t[I_{II}(I^x, I^0) + I_{II}(I^0, I^x)] \tag{142}$$

$$D_{Ip_e}p_e^x = (1-\theta)\delta t[I_{p_e}(p_e^x)] \tag{143}$$

$$R_{IU}U^x = \phi\,\delta t[I_{IU}(I, U^x)] \tag{144}$$

$$R_{IV}V^x = \phi\,\delta t[I_{\psi V}(\psi, V^x)] \tag{145}$$

$$R_{I\chi}\chi^x = \phi\,\delta t[I_{I\chi}(I, \chi^x)] \tag{146}$$

$$Q_{IU}U^x = -\phi\,\delta t[I_{IU}(I, U^x)] + \delta t[I_{IU}(I^0, U^x)] \tag{147}$$

$$Q_{IV}V^x = -\phi\,\delta t[I_{\psi V}(\psi, V^x)] + \delta t[I_{\psi U}(\psi^0, V^x)] \tag{148}$$

$$Q_{I\chi}\chi^x = -\phi\,\delta t[I_{I\chi}(I, \chi^x)] + \delta t[I_{I\chi}(I^0, \chi^x)] \tag{149}$$

*C.2. Matrix element component terms*

The terms in the above equations are categorized and defined in the following sections. Each term has been integrated by parts to arrive at the simplest expression for which the order of differentiation on the trial function is roughly equal to that on the physical fields. The integrations by parts of tensor quantities are aided by use of the following identities, which hold for any symmetric tensor $\Pi$:

$$R^2 v\nabla\varphi\cdot\nabla\times(\nabla\cdot\Pi) = R^2 v_Z\nabla\varphi\cdot\Pi\cdot\nabla\varphi - \nabla v\cdot\Pi\cdot\nabla Z + R\nabla\varphi\cdot[\nabla\nabla(vR)\dot{\times}\Pi] + \nabla\cdot\mathbf{A}_1 \tag{150}$$

$$-R^2 v\nabla\varphi\cdot(\nabla\cdot\Pi) = R^2\nabla v\cdot\Pi\cdot\nabla\varphi + \nabla\cdot\mathbf{A}_2 \tag{151}$$

$$-v\nabla\cdot(\nabla\cdot\Pi) = -\nabla\nabla v : \Pi + \nabla\cdot\mathbf{A}_3 \tag{152}$$

where

$$\mathbf{A}_1 = -R^2 v\nabla\varphi\times(\nabla\cdot\Pi) - R\Pi\cdot[\nabla\varphi\times\nabla(Rv)] + v\Pi\cdot\nabla z$$
$$\mathbf{A}_2 = -R^2 v\Pi\cdot\nabla\varphi$$
$$\mathbf{A}_3 = \nabla v\cdot\Pi - v\nabla\cdot\Pi.$$

In order to simplify the notation of the following terms, $A \equiv B$ is defined to mean $A = \int dA\; B$.

*C.2.1. Magnetohydrodynamic terms*

The terms in this section are the basic magnetohydrodynamic terms in the two-fluid equations, which do not depend on any specific choice of closure. These terms include convection, internal forces (pressure, Lorentz force), and electromagnetic induction.

$$
\begin{aligned}
&N_n(n) \equiv vn \\
&N_{nU}(n,U) \equiv v[U,n] \\
&N_{n\chi}(n,\chi) \equiv n\langle v,\chi\rangle - \nabla\cdot(vn\nabla\chi) \\
&N_{nD_n}(n,D_n) \equiv -D_n\langle v,n\rangle + \nabla\cdot(vD_n\nabla n) \\
&U_{Un}(U,n) \equiv -\tfrac{1}{R^2}n\langle R^2 v,U\rangle + \nabla\cdot(vn\nabla U) \\
&U_{\chi n}(\chi,n) \equiv -R^2 v[n,\chi] \\
&U_{UUn}(U,U,n) \equiv \tfrac{1}{R^2}n\Delta^* U[R^2 v,U] + \tfrac{1}{2R^2}\langle U,U\rangle[R^2 v,n] - [vn\Delta^* U,U] - \left[\tfrac{1}{2}v\langle U,U\rangle,n\right] \\
&U_{VVn}(V,V,n) \equiv \tfrac{1}{2R^2}[v,R^2]VVn - \left[\tfrac{1}{R}vnVV,R\right] \\
&U_{U\chi n}(U,\chi,n) \equiv \tfrac{1}{R^2}n\Delta^* U\langle R^2 v,\chi\rangle - [U,\chi][R^2 v,n] - \nabla\cdot(vn\Delta^* U\nabla\chi) - [R^2 v[\chi,U],n] \\
&U_{\chi\chi n}(\chi,\chi,n) \equiv \tfrac{1}{2}\langle\chi,\chi\rangle[R^2 v,n] - \left[\tfrac{1}{2}R^2 v\langle\chi,\chi\rangle,n\right] \\
&U_{\psi\psi}(\psi,\psi) \equiv -\tfrac{1}{R^2}[R^2 v,\psi]\Delta^*\psi - [\psi,v\Delta^*\psi] \\
&U_{II}(I,I) \equiv -R^2 vI\left[I,\tfrac{1}{R^2}\right] \\
&V_{Vn}(V,n) \equiv vnV \\
&V_{UVn}(U,V,n) \equiv vn[U,V] \\
&V_{V\chi n}(V,\chi,n) \equiv -vn\langle\chi,V\rangle \\
&V_{\psi I}(\psi,I) \equiv v[I,\psi] \\
&X_{Un}(U,n) \equiv v[n,U] \\
&X_{\chi n}(\chi,n) \equiv -n\langle v,\chi\rangle + \nabla\cdot(vn\nabla\chi) \\
&X_p(p) \equiv -v\nabla^2 p \\
&X_{UUn}(U,U,n) \equiv -\tfrac{1}{R^2}n\Delta^* U\langle v,U\rangle + \tfrac{1}{2}n\langle v,\tfrac{\langle U,U\rangle}{R^2}\rangle + \nabla\cdot\left(\tfrac{1}{R^2}vn\Delta^* U\nabla U\right) - \nabla\cdot\left[\tfrac{1}{2}vn\nabla\left(\tfrac{1}{R^2}\langle U,U\rangle\right)\right] \\
&X_{VVn}(V,V,n) \equiv \tfrac{1}{2}nVV\langle\tfrac{1}{R^2},v\rangle + \nabla\cdot\left(\tfrac{1}{R^3}vnVV\nabla R\right) \\
&X_{U\chi n}(U,\chi,n) \equiv (n\nabla^2 v + \langle n,v\rangle)[U,\chi] + n\Delta^* U[v,\chi] + \nabla\cdot(vn\nabla[U,\chi] - n[U,\chi]\nabla v) - [vn\Delta^* U,\chi] \\
&X_{\chi\chi n}(\chi,\chi,n) \equiv \tfrac{1}{2}n\langle v,\langle\chi,\chi\rangle\rangle - \nabla\cdot\left(\tfrac{1}{2}vn\nabla\langle\chi,\chi\rangle\right) \\
&X_{\psi\psi}(\psi,\psi) \equiv \tfrac{1}{R^2}\Delta^*\psi\langle v,\psi\rangle - \nabla\cdot\left(\tfrac{1}{R^2}v\Delta^*\psi\nabla\psi\right) \\
&X_{II}(I,I) \equiv \tfrac{1}{R^2}I\langle v,I\rangle - \nabla\cdot\left(\tfrac{1}{R^2}vI\nabla I\right) \\
&\Psi_\psi(\psi) \equiv v\psi \\
&\Psi_{\psi U}(\psi,U) \equiv v[U,\psi] \\
&\Psi_{\psi\chi}(\psi,\chi) \equiv -v\langle\chi,\psi\rangle \\
&\Psi_{\psi I}(\psi,I) \equiv d_i v\tfrac{1}{n}[\psi,I] \\
&I_I(I) \equiv vI \\
&I_{IU}(I,U) \equiv R^2 v\left[U,\tfrac{I}{R^2}\right] \\
&I_{\psi V}(\psi,V) \equiv R^2 v\left[\tfrac{V}{R^2},\psi\right] \\
&I_{I\chi}(I,\chi) \equiv \tfrac{I}{R^2}\langle R^2 v,\chi\rangle - \nabla\cdot(vI\nabla\chi) \\
&I_{\psi\psi}(\psi,\psi) \equiv d_i\tfrac{\Delta^*\psi}{R^2 n}[\psi,R^2 v] + \left[d_i\tfrac{1}{n}v\Delta^*\psi,\psi\right] \\
&I_{II}(I,I) \equiv d_i R^2 vI\left[\tfrac{1}{R^2 n},I\right] \\
&I_{p_e}(p_e) \equiv d_i R^2 v\left[\tfrac{1}{n},p_e\right] \\
&P_p(p) \equiv vp \\
&P_{pU}(p,U) \equiv v[U,p] \\
&P_{p\chi}(p,\chi) \equiv \Gamma p\langle v,\chi\rangle + (\Gamma-1)v\langle p,\chi\rangle - \nabla\cdot(\Gamma vp\nabla\chi) \\
&P_{p_eI}(p_e,I) \equiv d_i\left(\tfrac{1}{n}v[p_e,I] + \Gamma vp_e\left[\tfrac{1}{n},I\right]\right)
\end{aligned}
\tag{153}
$$

$$
\tag{154}
$$

$$
\tag{155}
$$

$$
\tag{156}
$$

$$
\tag{157}
$$

$$
\tag{158}
$$

$$
\tag{159}
$$

*Terms arising from* $\mathcal{L}(\mathbf{u})$. The following terms arise from the ideal MHD operator term $\mathcal{L}(\mathbf{u})$ in Eq. (21).

$$
\begin{aligned}
&U_{U\psi\psi}(U,\psi,\psi) \equiv \tfrac{1}{R^2}\langle [R^2 v,\psi],[U,\psi]\rangle - \tfrac{1}{R^2}[R^2 v,[U,\psi]]\Delta^*\psi + [v\Delta^*[U,\psi],\psi] + [v\Delta^*\psi,[U,\psi]] - \nabla\cdot\left(\tfrac{1}{R^2}[R^2 v,\psi]\nabla[U,\psi]\right)\\
&U_{UII}(U,I,I) \equiv [R^2,v]I\left[U,\tfrac{I}{R^2}\right] - \left[R^2, vI\left[U,\tfrac{I}{R^2}\right]\right]\\
&U_{V\psi I}(V,\psi,I) \equiv [R^2,v]I\left[\tfrac{V}{R^2},\psi\right] - \left[R^2, vI\left[\tfrac{V}{R^2},\psi\right]\right]
\end{aligned}
\tag{160}
$$

$$
\begin{aligned}
&U_{\chi\psi\psi}(\chi,\psi,\psi) \equiv -\tfrac{1}{R^2}\langle [R^2 v,\psi],\langle\chi,\psi\rangle\rangle + \tfrac{1}{R^2}[R^2 v,\langle\chi,\psi\rangle]\Delta^*\psi - [v\Delta^*\langle\chi,\psi\rangle,\psi] - [v\Delta^*\psi,\langle\chi,\psi\rangle] + \nabla\cdot\left(\tfrac{1}{R^2}[R^2 v,\psi]\nabla\langle\chi,\psi\rangle\right)\\
&U_{\chi II}(\chi,I,I) \equiv \tfrac{1}{R^2}[v,R^2]I(I\Delta^*\chi + \langle I,\chi\rangle) - \left[\tfrac{1}{R^2}vI(I\Delta^*\chi + \langle I,\chi\rangle),R^2\right]\\
&V_{U\psi I}(U,\psi,I) \equiv [v,U][I,\psi] + \tfrac{1}{R^2}I[U,R^2][v,\psi] + \left[R^2 v\left[U,\tfrac{I}{R^2}\right],\psi\right] + [I,v[U,\psi]]\\
&V_{V\psi\psi}(V,\psi,\psi) \equiv -[v,\psi][V,\psi] - \tfrac{1}{R^2}V[\psi,R^2][v,\psi] + \left[R^2 v\left[\tfrac{V}{R^2},\psi\right],\psi\right]\\
&V_{\chi I I}(\chi,\psi,I) \equiv [v,\psi](I\Delta^*\chi + \langle I,\chi\rangle) - \langle\chi,\psi\rangle[v,I] - [v(I\Delta^*\chi + \langle I,\chi\rangle),\psi] - [I,v\langle\chi,\psi\rangle]\\
&X_{Up}(U,p) \equiv -\nabla^2 v[U,p] + \nabla\cdot([U,p]\nabla v - v\nabla[U,p])\\
&X_{\chi p}(\chi,p) \equiv \nabla^2 v(\Gamma p\nabla^2\chi + \langle p,\chi\rangle) + \nabla\cdot[v\nabla(\Gamma p\nabla^2\chi + \langle p,\chi\rangle) - (\Gamma p\nabla^2\chi + \langle p,\chi\rangle)\nabla v]\\
&X_{U\psi\psi}(U,\psi,\psi) \equiv \tfrac{1}{R^2}\langle v,[U,\psi]\rangle\Delta^*\psi - \tfrac{1}{R^2}\langle\langle v,\psi\rangle,[U,\psi]\rangle - \nabla\cdot\left(\tfrac{1}{R^2}v\Delta^*\psi\nabla[U,\psi] + \tfrac{1}{R^2}v\Delta^*[U,\psi]\nabla\psi - \tfrac{1}{R^2}\langle v,\psi\rangle\nabla[U,\psi]\right)\\
&X_{UII}(U,I,I) \equiv -\nabla^2 vI\left[U,\tfrac{I}{R^2}\right] + \nabla\cdot\left[I\left[U,\tfrac{I}{R^2}\right]\nabla v - \tfrac{1}{R^2}v\nabla\left(R^2 I\left[U,\tfrac{I}{R^2}\right]\right)\right]\\
&X_{V\psi I}(V,\psi,I) \equiv -\Delta^* vI\left[\tfrac{V}{R^2},\psi\right] + \nabla\cdot\left[I\left[\tfrac{V}{R^2},\psi\right]\nabla v - \tfrac{1}{R^2}v\nabla\left(R^2 I\left[\tfrac{V}{R^2},\psi\right]\right)\right]\\
&X_{\chi\psi\psi}(\chi,\psi,\psi) \equiv -\tfrac{1}{R^2}\langle v,\langle\chi,\psi\rangle\rangle\Delta^*\psi + \tfrac{1}{R^2}\langle\langle v,\psi\rangle,\langle\chi,\psi\rangle\rangle\nabla\cdot\left(\tfrac{1}{R^2}v\Delta^*\psi\nabla\langle\chi,\psi\rangle + \tfrac{1}{R^2}v\Delta^*\langle\chi,\psi\rangle\nabla\psi - \tfrac{1}{R^2}\langle v,\psi\rangle\nabla\langle\chi,\psi\rangle\right)\\
&X_{\chi II}(\chi,I,I) \equiv \tfrac{1}{R^2}\nabla^2 vI(I\nabla^2\chi + \langle I,\chi\rangle) + \nabla\cdot\left\{\tfrac{1}{R^2}v\nabla[I(I\nabla^2\chi + \langle I,\chi\rangle)] - \tfrac{1}{R^2}\nabla vI(I\nabla^2\chi + \langle I,\chi\rangle)\right\}
\end{aligned}
\tag{161}
$$

$$
\begin{aligned}
&X_{Up}(U,p) \equiv -\nabla^2 v[U,p] + \nabla\cdot([U,p]\nabla v - v\nabla[U,p])\\
&X_{\chi p}(\chi,p) \equiv \nabla^2 v(\Gamma p\nabla^2\chi + \langle p,\chi\rangle) + \nabla\cdot[v\nabla(\Gamma p\nabla^2\chi + \langle p,\chi\rangle) - (\Gamma p\nabla^2\chi + \langle p,\chi\rangle)\nabla v]\\
&X_{U\psi\psi}(U,\psi,\psi) \equiv \tfrac{1}{R^2}\langle v,[U,\psi]\rangle\Delta^*\psi - \tfrac{1}{R^2}\langle\langle v,\psi\rangle,[U,\psi]\rangle - \nabla\cdot\left(\tfrac{1}{R^2}v\Delta^*\psi\nabla[U,\psi] + \tfrac{1}{R^2}v\Delta^*[U,\psi]\nabla\psi - \tfrac{1}{R^2}\langle v,\psi\rangle\nabla[U,\psi]\right)\\
&X_{UII}(U,I,I) \equiv -\nabla^2 vI\left[U,\tfrac{I}{R^2}\right] + \nabla\cdot\left[I\left[U,\tfrac{I}{R^2}\right]\nabla v - \tfrac{1}{R^2}v\nabla\left(R^2 I\left[U,\tfrac{I}{R^2}\right]\right)\right]\\
&X_{V\psi I}(V,\psi,I) \equiv -\Delta^* vI\left[\tfrac{V}{R^2},\psi\right] + \nabla\cdot\left[I\left[\tfrac{V}{R^2},\psi\right]\nabla v - \tfrac{1}{R^2}v\nabla\left(R^2 I\left[\tfrac{V}{R^2},\psi\right]\right)\right]\\
&X_{\chi\psi\psi}(\chi,\psi,\psi) \equiv -\tfrac{1}{R^2}\langle v,\langle\chi,\psi\rangle\rangle\Delta^*\psi + \tfrac{1}{R^2}\langle\langle v,\psi\rangle,\langle\chi,\psi\rangle\rangle\nabla\cdot\left(\tfrac{1}{R^2}v\Delta^*\psi\nabla\langle\chi,\psi\rangle + \tfrac{1}{R^2}v\Delta^*\langle\chi,\psi\rangle\nabla\psi - \tfrac{1}{R^2}\langle v,\psi\rangle\nabla\langle\chi,\psi\rangle\right)\\
&X_{\chi II}(\chi,I,I) \equiv \tfrac{1}{R^2}\nabla^2 vI(I\nabla^2\chi + \langle I,\chi\rangle) + \nabla\cdot\left\{\tfrac{1}{R^2}v\nabla[I(I\nabla^2\chi + \langle I,\chi\rangle)] - \tfrac{1}{R^2}\nabla vI(I\nabla^2\chi + \langle I,\chi\rangle)\right\}
\end{aligned}
\tag{162}
$$

### C.2.2. Collisional forces

Assuming the collisional force **R** is of the form given by Eq. (8) (which neglects the thermal force), the contributions to the scalar equations due to this force are given by

$$
\begin{aligned}
&\Psi_{\psi\eta}(\psi) \equiv v\eta\Delta^*\psi\\
&I_{I\eta}(I) \equiv -\frac{1}{R^2}\eta\langle R^2 v,I\rangle + \nabla\cdot(v\eta\nabla I)\\
&P_{\psi\psi\eta}(\psi,\psi) \equiv (\Gamma-1)\frac{1}{R^2}v\eta\Delta^*\psi\Delta^*\psi\\
&P_{II\eta}(I,I) \equiv (\Gamma-1)\frac{1}{R^2}v\eta\langle I,I\rangle.
\end{aligned}
\tag{163}
$$

### C.2.3. Gravity

These terms are obtained assuming a gravitational force of the form given by Eq. (16). (Note that here the subscripts on $g$ denote vector components, not derivatives.)

$$
\begin{aligned}
&U_{n\mathbf{g}}(n) \equiv g_R v[n,R] - g_Z R v\langle n,R\rangle\\
&X_{n\mathbf{g}}(n) \equiv \frac{n}{R^2}(g_R\langle v,R\rangle + g_Z R[v,R]).
\end{aligned}
\tag{164}
$$

*Gravitational terms arising from analytic density advance*. The numerical stability of simulations of gravitational modes may be greatly improved by Taylor expanding $n$ in the gravity term of the velocity advance and using the analytic form of $\dot{n}$ to eliminate the advanced-time occurrences of $n$ in that term (in the same manner as **B** is treated throughout the velocity advance). This procedure leads to the following terms:

$$
\begin{aligned}
&U_{Un\mathbf{g}}(U,n) \equiv -[n,U]\left(\tfrac{1}{R}g_Z\langle R^2 v,R\rangle - \tfrac{1}{R^2}g_R[v,R]\right) + \nabla\cdot(Rvg_Z[n,U]\nabla R) - [vg_R[n,U],R]\\
&U_{\chi n\mathbf{g}}(\chi,n) \equiv -(n\nabla^2\chi + \langle n,\chi\rangle)\left(\tfrac{1}{R}g_Z\langle R^2 v,R\rangle - \tfrac{1}{R^2}g_R[v,R]\right) + \nabla\cdot[vRg_Z(n\nabla^2\chi + \langle n,\chi\rangle)\nabla R] - [vg_R(n\nabla^2\chi + \langle n,\chi\rangle),R]
\end{aligned}
\tag{165}
$$

$$
\begin{aligned}
&X_{Un\mathbf{g}}(U,n) \equiv [U,n]\left(Rg_Z[v,R] + \tfrac{1}{R^2}g_R\langle v,R\rangle\right) - [Rvg_Z[U,n],R] - \nabla\cdot\left[\tfrac{1}{R^2}vg_R[U,n]\nabla R\right]\\
&X_{\chi n\mathbf{g}}(\chi,n) \equiv -(n\nabla^2\chi + \langle n,\chi\rangle)\left(Rg_Z[v,R] + \tfrac{1}{R^2}g_R\langle v,R\rangle\right) - [Rvg_Z(n\nabla^2\chi + \langle n,\chi\rangle),R] - \nabla\cdot\left[\tfrac{1}{R^2}vg_R(n\nabla^2\chi + \langle n,\chi\rangle)\nabla R\right].
\end{aligned}
\tag{166}
$$

*C.2.4. Heat flux terms*

These terms are obtained assuming a heat flux density of the form given by Eq. (15).

$$\begin{aligned}
&P_{\kappa_\circ}(\kappa, T) \equiv -(\Gamma-1)\nu\kappa_\circ\nabla^2 T \\
&P_{\kappa_\parallel}(\kappa_\parallel, T, \psi, \psi, B^{-2}) \equiv -(\Gamma-1)\kappa_\parallel \frac{1}{B^2}[\psi, \nu][\psi, T] + \nabla\cdot[(\Gamma-1)\nu\kappa_\parallel \mathbf{bb}\cdot\nabla T] \\
&P_{\kappa_\wedge}(\kappa_\wedge, T, I, B^{-2}) \equiv (\Gamma-1)\kappa_\wedge \frac{I}{B}[\nu, T] + \nabla\cdot[(\Gamma-1)\nu\kappa_\wedge \mathbf{b}\times\nabla T]
\end{aligned} \tag{167}$$

where

$$B^2 = \frac{1}{R^2}[\langle\psi,\psi\rangle + I^2].$$

*C.2.5. Particle Source*

The particle source term is:

$$N_\sigma(\sigma) \equiv \nu\sigma. \tag{168}$$

The contributions to the momentum equation due to the particle source are:

$$\begin{aligned}
&U_{U\sigma}(U,\sigma) \equiv \frac{1}{R^2}\langle R^2\nu, U\rangle\sigma + \nabla\cdot(\nu\sigma\nabla U) \\
&U_{\chi\sigma}(\chi,\sigma) \equiv -[R^2\nu,\chi]\sigma + [\chi, R^2\nu\sigma] \\
&V_{V\sigma}(V,\sigma) \equiv -\nu V\sigma \\
&X_{U\sigma}(U,\sigma) \equiv [\nu, U]\sigma + [U, \nu\sigma] \\
&X_{\chi\sigma}(\chi,\sigma) \equiv \langle\nu,\chi\rangle\sigma + \nabla\cdot(\nu\sigma\nabla\chi)
\end{aligned} \tag{169}$$

The contributions to the pressure equation do to the particle source are:

$$\begin{aligned}
&P_\sigma \equiv P_{UU\sigma} + P_{VV\sigma} + P_{\chi\chi\sigma} + P_{U\chi\sigma} \\
&P_{UU\sigma}(U,U,\sigma) \equiv \frac{1}{2R^2}\nu\sigma\langle U, U\rangle \\
&P_{VV\sigma}(V,V,\sigma) \equiv \frac{1}{2R^2}\nu\sigma V^2 \\
&P_{\chi\chi\sigma}(\chi,\chi,\sigma) \equiv \frac{1}{2}\nu\sigma\langle\chi,\chi\rangle \\
&P_{\sigma U\chi}(U,\chi,\sigma) \equiv \nu\sigma[\chi, U]
\end{aligned} \tag{170}$$

*C.2.6. Viscosity*

The viscous terms are each the sum of the isotropic, parallel, and gyroviscous contributions:

$$A_{B\Pi}(B) = A_{B\Pi_\circ}(B) + A_{B\Pi_\parallel}(B) + A_{B\Pi_\wedge}(B)$$

where $A$ and $B$ are each one of $\{U, V, \chi\}$. Each contribution is described in the following sections.

*C.2.6.1. Isotropic viscosity.* These terms result from isotropic viscosity of the form given by Eq. (12).

$$\begin{aligned}
&U_{U\Pi_\circ}(U) \equiv \frac{1}{R^2}[(\langle\mu, R^2\nu\rangle + \mu\Delta^*(R^2\nu))\Delta^* U + \nabla^2\mu\langle R^2\nu, U\rangle + \Delta^*(R^2\nu)\langle\mu, U\rangle] \\
&U_{\chi\Pi_\circ}(\chi) \equiv -\nabla^2(R^2\nu)[\mu,\chi] - \Delta^*\mu[R^2\nu,\chi] - \frac{1}{R^2}\Delta^*(R^2\chi)[R^2\nu,\mu] \\
&V_{V\Pi_\circ}(V) \equiv [\langle\nu,\mu\rangle + \frac{1}{R^2}\mu\Delta^*(R^2\nu)]V \\
&X_{U\Pi_\circ}(U) \equiv \nabla^2\nu[\mu, U] + \nabla^2\mu[\nu, U] + \Delta^* U[\nu,\mu] \\
&X_{\chi\Pi_\circ}(\chi) \equiv \nabla^2\nu\langle\mu,\chi\rangle + \nabla^2\mu\langle\nu,\chi\rangle + 2\mu_c\nabla^2\nu\nabla^2\chi
\end{aligned} \tag{171}$$

*C.2.6.2. Parallel viscosity.* These terms are obtained assuming a parallel viscosity of the form given in Eq. (10). These equations were obtained using Eqs. (150)–(152). For compactness, derivatives are written as subscripts in the following expressions (i.e. $\nu_Z = \partial_Z\nu$).

Each term takes the form

$$A_{B\Pi_\parallel}(B) \equiv \mu_\parallel D_A S_B \tag{172}$$

where $A$ and $B$ are each one of $\{U, V, \chi\}$.

$$D_U = \frac{3}{B^2}\left\{-\frac{1}{2}R^2\left[v, \frac{\langle\psi,\psi\rangle}{R^2}\right] + \langle\psi,[v,\psi]\rangle - \frac{1}{R^2}I^2 v_Z - \frac{2}{R^2}[v_Z(\psi_Z^2 - \psi_R^2) + 2v_R\psi_R\psi_Z]\right\}$$

$$D_V = -3\frac{I}{B^2}[v,\psi]$$

$$D_X = -\nabla^2 v\left(1 - 3\frac{\langle\psi,\psi\rangle}{R^2B^2}\right) + \frac{3}{R^2B^2}\left(\frac{1}{2}R^2\langle v, \frac{\langle\psi,\psi\rangle}{R^2}\rangle - \langle\psi,\langle v,\psi\rangle\rangle + \frac{1}{R}I^2 v_R\right)$$

$$S_U = \frac{1}{R^2B^2}\left(-\frac{1}{2}R^2\left[U, \frac{\langle\psi,\psi\rangle}{R^2}\right] + \langle\psi,[U,\psi]\rangle - \frac{1}{R^2}I^2 U_Z\right)$$

$$S_V = -\frac{I}{B^2}\left[\psi, \frac{V}{R^2}\right]$$

$$S_\chi = \frac{1}{R^2B^2}\left(\frac{1}{2}R^2\langle\chi, \frac{\langle\psi,\psi\rangle}{R^2}\rangle - \langle\psi,\langle\chi,\psi\rangle\rangle + \frac{1}{R}I^2\chi_R + \nabla^2\chi\langle\psi,\psi\rangle\right) - \frac{1}{3}\nabla^2\chi$$

*C.2.6.3. Gyroviscosity.* These terms are obtained using Eqs. (150)–(152) assuming a gyroviscosity of the form given by Eq. (11).

$$U_{U\Pi_\wedge}(U) \equiv \frac{p_i I}{2R^3B^2}\times\left\{\begin{array}{l}\left(1+\frac{3}{2}\frac{\langle\psi,\psi\rangle}{R^2B^2}\right)\left[\begin{array}{c}([R^3v_Z]_Z - [R^3v_R]_R)\left(\left[\frac{U_R}{R}\right]_Z + \left[\frac{U_Z}{R}\right]_R\right)\\ -([R^3v_R]_Z + [R^3v_Z]_R)\left(\left[\frac{U_Z}{R}\right]_Z - \left[\frac{U_R}{R}\right]_R\right)\end{array}\right]\\ +\frac{9}{2RB^2}\left[\begin{array}{c}(\psi_Z^2 - \psi_R^2)\left(\begin{array}{c}Rv_Z\left[\left(\frac{U_Z}{R}\right)_Z - \left(\frac{U_R}{R}\right)_R\right]\\ -\frac{1}{R^3}U_Z[(R^3v_Z)_Z - (R^3v_R)_R]\end{array}\right)\\ +2\psi_R\psi_Z\left(\begin{array}{c}Rv_Z\left[\left(\frac{U_R}{R}\right)_Z + \left(\frac{U_Z}{R}\right)_R\right]\\ -\frac{1}{R^3}U_Z[(R^3v_R)_Z + (R^3v_Z)_R]\end{array}\right)\end{array}\right]\end{array}\right\}$$

$$U_{V\Pi_\wedge}(V) \equiv \frac{p_i}{B^2}\times\left\{\begin{array}{l}\frac{1}{4R^2}\left(1-\frac{3I^2}{B^2R^2}\right)\left(\left\langle\frac{V}{R^2}, R^4[\psi,v]\right\rangle - \left\langle\psi, R^4\left[v,\frac{V}{R^2}\right]\right\rangle + \frac{1}{R^2}\left[v, R^6\left\langle\frac{V}{R^2},\psi\right\rangle\right]\right)\\ -\frac{3}{4B^2}\left[\psi,\frac{V}{R^2}\right]\left(2\langle\psi,\langle\psi,v\rangle\rangle - R^2\left\langle v,\frac{\langle\psi,\psi\rangle}{R^2}\right\rangle - \Delta^* v\langle\psi,\psi\rangle + 6\psi_Z[v,\psi]\right)\\ +\frac{9I^2}{2R^2B^2}v_Z\left\langle\psi,\frac{V}{R^2}\right\rangle\end{array}\right\}$$

$$U_{\chi\Pi_\wedge}(\chi) \equiv \frac{p_i I}{2R^3B^2}\times\left\{\begin{array}{l}[(\chi_{RR}-\chi_{ZZ})([R^3v_R]_R - [R^3v_Z]_Z) + 2\chi_{RZ}([R^3v_R]_Z + [R^3v_Z]_R)]\\ +\frac{3}{R^2B^2}\left[\begin{array}{c}(\Delta^*\chi[\psi_Z^2 - \psi_R^2] - \chi_{ZZ}\psi_Z^2 + \chi_{RR}\psi_R^2)\\ \times([R^3v_R]_R - [R^3v_Z]_Z)\\ +2\chi_{RZ}\left(\psi_Z^2[R^3v_R]_Z + \psi_R^2[R^3v_Z]_R\right)\\ -2\psi_R\psi_Z\left(\begin{array}{c}[\chi_{ZZ} - \frac{1}{R}\chi_R][R^3v_R]_Z\\ +[\chi_{RR} - \frac{1}{R}\chi_R][R^3v_Z]_R\end{array}\right)\end{array}\right]\end{array}\right\}$$

$$V_{U\Pi_\wedge}(U) \equiv -\frac{p_i}{4RB^2}\times\left\{\begin{array}{l}\left(1-3\frac{I^2}{R^2B^2}\right)\left(\begin{array}{c}\langle\psi,R[U,v]\rangle + \langle v,R[U,\psi]\rangle\\ -\frac{1}{R^3}\left[U,R^4\langle v,\psi\rangle\right] + U_R[v,\psi] + \frac{2}{R}\psi_Z\langle v,U\rangle\end{array}\right)\\ +\frac{3}{RB^2}[\psi,v]\left(\begin{array}{c}2\langle\psi,\langle U,\psi\rangle\rangle - \Delta^* U\langle\psi,\psi\rangle\\ -\frac{1}{R^2}\langle U,R^2\langle\psi,\psi\rangle\rangle + [\psi,R^2][\psi,U]\end{array}\right)\\ -18\frac{I^2}{R^2B^2}[U,R]\langle v,\psi\rangle\end{array}\right\}$$

$$
\begin{aligned}
V_{V\Pi_\wedge}(V) &\equiv -\frac{p_i I R^2}{B^2}\left(1-\frac{3}{2}\frac{\langle\psi,\psi\rangle}{R^2B^2}\right)[v,\frac{V}{R^2}]V_{\chi\Pi_\wedge}(\chi)\\
&\equiv -\frac{p_i}{B^2}\times\left\{\begin{array}{l}\frac{1}{4}\left(\frac{1}{R^2}\langle\chi,R^2\langle v,\psi\rangle\rangle-\langle v,\langle\chi,\psi\rangle\rangle-\langle\psi,\langle v,\chi\rangle\rangle\right)\\ +\frac{3}{2RB^2}[\psi,v]\left(\langle\psi,R[\chi,\psi]\rangle-\frac{1}{2}R[\chi,\langle\psi,\psi\rangle]\right)\\ +\frac{3}{4}\frac{I^2}{R^2B^2}\left(\langle\psi,\langle\chi,v\rangle\rangle+\langle v,\langle\chi,\psi\rangle\rangle-\langle\chi,\langle v,\psi\rangle\rangle-2\Delta^*\chi\langle v,\psi\rangle\right)\end{array}\right\}X_{U\Pi_\wedge}(U)\\
&\equiv -\frac{p_i I}{2R^2B^2}\times\left\{\begin{array}{l}\langle\langle v,U\rangle\rangle-R^2[[v,U]]+\frac{1}{R}\left[U_R(v_{ZZ}-v_{RR})-2U_Zv_{RZ}-\frac{1}{R}U_Rv_R\right]\\ +\frac{3}{RB^2}\left[\begin{array}{c}\left(\left[\frac{U_Z}{R}\right]_Z-\left[\frac{U_R}{R}\right]_R\right)\left(v_{ZZ}\psi_R^2-v_{RR}\psi_Z^2+\frac{1}{R}v_R[\psi_Z^2-\psi_R^2]\right)\\ +2v_{RZ}\left(\left[\frac{U_R}{R}\right]_Z\psi_R^2+\left[\frac{U_Z}{R}\right]_R\psi_Z^2-\frac{1}{R^2}U_Z[\psi_Z^2-\psi_R^2]\right)\\ -2\psi_R\psi_Z\left(\begin{array}{c}\left[\frac{U_R}{R}\right]_Zv_{RR}+\left[\frac{U_Z}{R}\right]_Rv_{ZZ}\\ -\frac{1}{R^2}U_Z[v_{ZZ}-v_{RR}]\\ -\frac{1}{R}v_R\left[\left(\frac{U_R}{R}\right)_Z+\left(\frac{U_Z}{R}\right)_R\right]\end{array}\right)\end{array}\right]\end{array}\right\}X_{V\Pi_\wedge}(V)\\
&\equiv -\frac{p_i}{4B^2}\times\left\{\begin{array}{l}\left(1-\frac{3}{R^2}\frac{I^2}{B^2}\right)\left(\frac{1}{R^2}\left\langle v,R^2\left\langle\frac{V}{R^2},\psi\right\rangle\right\rangle-\left\langle\psi,\left\langle\frac{V}{R^2},v\right\rangle\right\rangle-\left\langle\frac{V}{R^2},\langle\psi,v\rangle\right\rangle\right)\\ +\frac{6}{B^2}\left[\psi,\frac{V}{R^2}\right]\left(\frac{1}{R}\langle\psi,R[v,\psi]\rangle-\frac{1}{2}[v,\langle\psi,\psi\rangle]\right)\\ -6\frac{I^2}{B^2}\left\langle\psi,\frac{V}{R^2}\right\rangle\left[\left(\frac{v_Z}{R^2}\right)_Z+\left(\frac{v_R}{R^2}\right)_R\right]\end{array}\right\}X_{\chi\Pi_\wedge}(\chi)\\
&\equiv \frac{p_i I}{B^2}\times\left\{\begin{array}{l}\left(1+\frac{3}{2R^2}\frac{\langle\psi,\psi\rangle}{B^2}\right)[\langle v,\chi\rangle]\\ +\frac{3}{2B^2}\left[\begin{array}{l}\left(-\frac{1}{2}[\chi,\langle\psi,\psi\rangle]+\frac{1}{R}\langle\psi,R[\chi,\psi]\rangle\right)\left(\left[\frac{v_R}{R^2}\right]_R+\left[\frac{v_Z}{R^2}\right]_Z\right)\\ -\left(-\frac{1}{2}[v,\langle\psi,\psi\rangle]+\frac{1}{R}\langle\psi,R[v,\psi]\rangle\right)\left(\left[\frac{\chi_R}{R^2}\right]_R+\left[\frac{\chi_Z}{R^2}\right]_Z\right)\end{array}\right]\end{array}\right\}
\end{aligned}
$$

*C.2.6.4. Viscous heating.* The contributions from viscous heating $-(\Pi:\nabla\mathbf{u})$ are

$$
\begin{aligned}
&P_{\Pi_\circ} = P_{\Pi_\circ UU}+P_{\Pi_\circ VV}+P_{\Pi_\circ\chi\chi}+P_{\Pi_\circ U\chi}\\
&P_{\Pi_\circ UU}(U,U)\equiv \nu\mu\left(\frac{1}{R^2}\Delta^*U\Delta^*U-\frac{1}{2}[[U,U]]-\frac{1}{R}\left[U,\frac{1}{R}U_Z\right]\right)\\
&P_{\Pi_\circ VV}(V,V)\equiv \nu\mu R^2\left\langle\frac{V}{R^2},\frac{V}{R^2}\right\rangle\\
&P_{\Pi_\circ\chi\chi}(\chi,\chi)\equiv 2\nu(\mu_c-\mu)\nabla^2\chi\nabla^2\chi-2\nu\mu\langle\langle\chi,\chi\rangle\rangle\\
&P_{\Pi_\circ U\chi}(U,\chi)\equiv -4\nu\mu\left([\langle U,\chi\rangle]-\left[U,\frac{1}{R}\chi_R\right]\right),\\
&P_{\Pi_\parallel}\equiv 3\mu_\parallel\left(\frac{1}{2}\mathbf{b}\cdot\mathsf{W}\cdot\mathbf{b}\right)^2\\
&P_{\Pi_\wedge}\equiv 0
\end{aligned}
\tag{173}
$$

where $\frac{1}{2}\mathbf{b}\cdot\mathsf{W}\cdot\mathbf{b}=S_U+S_V+S_\chi$, as defined in Section C.2.6.2. Note that gyroviscosity is not dissipative, and does not contribute to viscous heating.

*C.2.7. Electron viscosity*

The contribution from electron viscous heating $(d_i\Pi_e:\nabla\frac{\mathbf{J}}{n})$ is

$$
P_{\Pi_e}\equiv \nu\lambda\left[n\left\langle\frac{\Delta^*\psi}{nR},\frac{\Delta^*\psi}{R}\right\rangle+\frac{1}{R^4}(\Delta^*\psi)^2+\frac{1}{R^2}\left(\langle\langle I,I\rangle\rangle-\frac{2}{R^2}I_R^2+\frac{1}{2}nR^4\left\langle\frac{1}{nr^2},\frac{\langle I,I\rangle}{R^2}\right\rangle\right)\right]
\tag{174}
$$

## References


[1] S.C. Jardin, J. Breslau, N. Ferraro, A high-order implicit finite element method for integrating the two-fluid magnetohydrodynamic equations in two dimensions, J. Comp. Phys. 226 (2) (2007) 2146–2174.

[2] M. Ono, S.M. Kaye, Y.-K.M. Peng, G. Barnes, W. Blanchard, M.D. Carter, J. Chrzanowski, L. Dudek, R. Ewig, D. Gates, R.E. Hatcher, T. Jarboe, S.C. Jardin, D. Johnson, R. Kaita, M. Kalish, C.E. Kessel, H.W. Kugel, R. Maingi, R. Majeski, J. Manickam, B. McCormack, J. Menard, D. Mueller, B.A. Nelson, B.E. Nelson, C. Neumeyer, G. Oliaro, F. Paoletti, R. Parsells, E. Perry, N. Pomphrey, S. Ramakrishnan, R. Raman, G. Rewoldt, J. Robinson, A.L. Roquemore, P. Ryan, S. Sabbagh, D. Swain, E.J. Synakowski, M. Viola, M. Willians, J.R. Wilson, N. Team, Exploration of spherical torus physics in the NSTX device, Nucl. Fusion 40 (3Y) (2000) 557–561.

[3] A.Y. Aydemir, Shear flows at the tokamak edge and their interaction with edge-localized modes, Phys. Plasmas 14.

[4] T.E. Stringer, Diffusion in toroidal plasmas with radial electric field, Phys. Rev. Lett 22 (15) (1969) 770–774.

[5] M.N. Rosenbluth, J.B. Taylor, Plasma diffusion and stability in toroidal systems, Phys. Rev. Lett. 23 (7) (1969) 367–370.

[6] A.A. Galeev, Influence of termperature perturbation on plasma diffusion in toroidal systems, ZhETF Pis. Red. 10 (7) (1969) 353–357.

[7] O.P. Pogutse, Classical diffusion of a plasma in toroidal systems, Nucl. Fusion 10 (1970) 399–403.

[8] A. Bondeson, D.J. Ward, Stabilization of external modes in tokamaks by resistive walls and plasma rotation, Phys. Rev. Lett. 72 (17) (1994) 2709–2712.
[9] A.M. Garofalo, E.J. Strait, L.C. Johnson, R.J.L. Haye, E.A. Lazarus, G.A. Navratil, M. Okabayashi, J.T. Scoville, T.S. Taylor, A.D. Turnbull, Sustained stabilization of resistive-wall mode by plasma rotation in the DIII-D tokamak, Phys. Rev. Lett. 89 (23) (2002) 235001.
[10] B. LaBombard, J.E. Rice, A.E. Hubbard, J.W. Hughes, M. Greenwald, J. Irby, Y. Lin, B. Lipschultz, E.S. Marmar, C.S. Pitcher, N. Smick, S.M. Wolfe, S.J. Wukitch, the Alcator Group, Transport-driven scrape-off-layer flows and the boundary conditions imposed at the magnetic separatrix in a tokamak plasma, Nucl. Fusion 44 (2004) 1047–1066.
[11] H. Biglari, P.H. Diamond, P.W. Terry, Influence of sheared poloidal rotation on edge turbulence, Phys. Fluids B 2 (1) (2001) 1–3.
[12] K.H. Burrell, Effects of $E \times B$ velocity shear and magnetic shear on turbulence and transport in magnetic confinement devices, Phys. Plasmas 4 (1997) 1499.
[13] J.B. Taylor, Relaxation of toroidal plasma and generation of reverse magnetic fields, Phys. Rev. Lett. 33 (19) (1974) 1139–1141.
[14] L.C. Steinhauer, A. Ashida, Nearby-fluids equilibria. I. Formalism and transition to single-fluid magnetohydrodynamics, Phys. Plasmas 13 (2006) 052513.
[15] G.N. Throumoulopoulos, H. Tasso, On Hall magnetohydrodynamics equilibria, Phys. Plasmas 13 (2006) 102504.
[16] S. Semenzato, R. Gruber, H.P. Zehrfeld, Commputation of symmetric ideal MHD flow equilibria, Comp. Phys. Rep. 1 (1984) 389.
[17] A.J. Beliën, M.A. Botchev, J.P. Goedbloed, B. van der Holst, R. Keppens, FINESSE: axisymmetric MHD equilibria with flow, J. Comp. Phys. 182 (1) (2002) 91–117.
[18] L. Guazzotto, R. Betti, J. Manikam, S. Kaye, Numerical study of tokamak equilibria with arbitrary flow, Phys. Plasmas 11 (2) (2004) 604–614.
[19] L. Guazzotto, R. Betti, Magnetohydrodynamics equilibria with toroidal and poloidal flow, Phys. Plasmas 12 (2005) 056107.
[20] J.A. Breslau, C.R. Sovinec, S.C. Jardin, An improved tokamak sawtooth benchmark for 3D nonlinear MHD, Comm. Comp. Phys. 4 (3) (2008) 647–658.
[21] A.Y. Aydemir, D.C. Barnes, Three-dimensional nonlinear incompressible MHD calculations, J. Comp. Phys. 53 (1) (1984) 100–123.
[22] N.M. Ferraro, S.C. Jardin, Finite element implementation of Braginskii's gyroviscous stress with application to the gravitational instability, Phys. Plasmas 13 (9) (2006) 092101.
[23] C. Sovinec, A. Glasser, T. Gianakon, D. Barnes, R. Nebel, S. Kruger, S. Plimpton, A. Tarditi, M. Chu, the NIMROD Team, Nonlinear magnetohydrodynamics with high-order finite elements, J. Comp. Phys. 195 (2004) 355.
[24] S.C. Jardin, A triangular finite element with first-derivative continuity applied to fusion MHD applications, J. Comp. Phys. 200 (2004) 133–152.
[25] S.I. Braginskii, Transport processes in a plasma, in: M.A. Leontovich (Ed.), Reviews of Plasma Physics, vol. 1, Consultants Bureau, New York, 1965, pp. 205–311.
[26] M.D. Rosen, J.M. Greene, Radial boundary layers in diffusing toroidal equilibria, Phys. Fluids 20 (9) (1977) 1466–1475.
[27] D.A. Dunavant, High degree efficient symmetrical gaussian quadrature rules for the triangle, Int. J. Numer. Methods Eng. 21 (1985) 1129–1148.
[28] D.S. Harned, D.D. Schnack, Semi-implicit method for long time scale magnetohydrodynamic computations in three dimensions, J. Comp. Phys. 65 (1) (1986) 57–70.
[29] L. Chacón, D.A. Knoll, A 2D high-$\beta$ Hall MHD implicit nonlinear solver, J. Comp. Phys. 188 (2) (2003) 573–592.
[30] E.J. Caramana, Derivation of implicit difference schemes by the method of differential approximation, J. Comp. Phys. 96 (1991) 484–493.
[31] R. Fitzpatrick, Scaling of forced magnetic reconnection in the Hall-magnetohydrodynamic Taylor problem, Phys. Plasmas 11 (3) (2004) 937–946.
[32] D. Pfirsch, A. Schlüter, Tech. Rep. MPI/PA/7/62, Max-Planck-Institut für Plasmaphysik, 1962.
[33] N.M. Ferraro, Non-ideal effects on the stability and transport of magnetized plasmas, Ph.D. thesis, Princeton University, Nov. 2008.
[34] A.B. Mikhailovskii, V.S. Tsypin, Transport equations and the gradient instabilities in a high pressure collisional plasma, Plasma Phys. 13 (1971) 785–798.
[35] R. Maingi, C.S. Shaing, S. Ku, T. Biewer, R. Maqueda, M. Bell, C. Bush, D. Gates, S. Kaye, H. Kugel, B. LeBlanc, J. Menard, D. Mueller, R. Raman, S. Sabbagh, V. Soukhanovskii, the NSTX Team, Effect of gas fuelling location on h-mode access in nstx, Plasma Phys. Control. Fusion 46 (2004) A305–A313.
[36] A.B. Hassam, R.M. Kulsrud, Time evolution of mass flows in a collisional tokamak, Phys. Fluids 21 (12) (1978) 2271–2279.